

## Regioselective Oxidation and Metalation of *meso*-Unsubstituted Azuliporphyrins

Venkata A. K. Adiraju, Gregory M. Ferrence and Timothy D. Lash

Department of Chemistry, Illinois State University, Normal, Illinois 61790-4160

E-mail: [tplash@ilstu.edu](mailto:tplash@ilstu.edu)

### Table of Contents

#### Page

S2-S5	Crystallographic Experimental Details
S6-S7	Summary of framework bond distances (Å) and angles (°) for <b>16a</b> , <b>17a</b> and <b>18b</b> (Table S1)
S8-S15	Selected views for the X-ray crystal structures of <b>16a</b> , <b>17a</b> and <b>18b</b> (Figures S1-S11)
S16-S26	Selected UV-vis spectra (Figures S12-S33)
S27-S64	Selected proton NMR, <sup>1</sup> H- <sup>1</sup> H COSY, HSQC, nOe difference <sup>1</sup> H NMR, DEPT-135 and carbon-13 NMR spectra (Figures S34-S86)
S64-S84	ESI MS (Figures S87-S106)

### Crystallographic Experimental Details of 16a·2 CHCl<sub>3</sub>

X-ray quality crystals of **16a·2 CHCl<sub>3</sub>** (C<sub>40</sub>H<sub>45</sub>N<sub>3</sub>O·2 CHCl<sub>3</sub>) were suspended in mineral oil at ambient temperature and a suitable crystal was selected. A mineral oil coated red needle thereby obtained of approximate dimensions 0.14 mm x 0.04 mm x 0.025 mm was mounted on a 50 μm MicroMesh MiTeGen Micromount and transferred to a Bruker AXS SMART APEX CCD X-ray diffractometer. The X-ray diffraction data were collected at 100(2) K using Mo-K<sub>α</sub> (λ = 0.71073 Å) radiation. A total of 3672 frames were collected. The total exposure time was 20.40 hours. The frames were integrated with the Bruker SAINT software package using a narrow-frame algorithm.<sup>S1</sup> The integration of the data yielded a total of 62093 reflections to a maximum θ angle of 27.55° (0.77 Å resolution), of which 8929 were independent (average redundancy 6.954, completeness = 99.8%,  $R_{\text{int}} = 9.38\%$ ,  $R_{\text{sig}} = 6.36\%$ ) and 5377 (60.22%) were observed with  $F_o^2 > 2\sigma(F_o^2)$ . The final triclinic cell constants of  $a = 8.3983(4)$  Å,  $b = 14.6292(6)$  Å,  $c = 16.7263(8)$  Å,  $\alpha = 92.703(3)^\circ$ ,  $\beta = 101.462(3)^\circ$ ,  $\gamma = 104.534(3)^\circ$ , volume = 1939.34(16) Å<sup>3</sup>, are based upon the refinement of the XYZ-centroids of 5264 reflections above 20  $\sigma(I)$  with  $4.996^\circ < 2\theta < 48.49^\circ$ . Limiting indices were as follows:  $-10 \leq h \leq 10$ ,  $-18 \leq k \leq 19$ ,  $-21 \leq l \leq 21$ . Data were corrected for absorption effects using the multi-scan method (SADABS).<sup>S1</sup> The ratio of minimum to maximum apparent transmission was 0.935 with minimum and maximum SADABS generated transmission coefficients of 0.6971 and 0.7456. Solution and data analysis were performed using the WinGX software package.<sup>S2</sup> The structure was solved and refined in the space group *P*-1 (no. 2) with *Z* = 2.<sup>S3</sup> The solution was achieved by charge-flipping methods using the program SUPERFLIP<sup>S4</sup> and the refinement was completed using the program SHELXL-2014/7.<sup>S5</sup> PLATON SQUEEZE<sup>S6</sup> was used to correct for the presence of one disordered chloroform molecule per main residue. 118 electrons in the unit cell is consistent with one CHCl<sub>3</sub> (58 electrons each; 116 electrons in a unit cell) per main residue. Aside from those removed by SQUEEZE, all non-H atoms were refined anisotropically. The two H atoms attached to nitrogen were identified in the difference Fourier and freely refined. Most other H atoms were identifiable in the difference Fourier; however, they were included in the refinement in the riding-model approximation (C--H = 0.95, 0.98, 0.99, and 1.00 Å for Ar--H, CH<sub>3</sub>, CH<sub>2</sub>, and CH;  $U_{\text{iso}}(\text{H}) = 1.2U_{\text{eq}}(\text{C})$  except for methyl groups, where  $U_{\text{iso}}(\text{H}) = 1.5U_{\text{eq}}(\text{C})$ ). Full-matrix least-squares refinement on  $F^2$  led to convergence,  $(\Delta/\sigma)_{\text{max}} = 0.000$ ,  $(\Delta/\sigma)_{\text{mean}} = 0.000$ , with  $R_1 = 0.0586$  and  $wR_2 = 0.1483$  for 5377 data with  $F_o^2 > 2\sigma(F_o^2)$  using 12 restraints and 441 parameters. A final difference Fourier synthesis showed features in the range of

$\Delta\rho_{max} = 0.892 \text{ e}/\text{\AA}^3$  to  $\Delta\rho_{min} = -0.878 \text{ e}/\text{\AA}^3$ . All residual electron density was within accepted norms and was deemed of no chemical significance. Molecular diagrams were generated using WinGX.<sup>S2</sup> CCDC-1496223 contains the supplementary crystallographic data for this structure. These data can be obtained free of charge from the Cambridge Crystallographic Data Centre via <https://summary.ccdc.cam.ac.uk/structure-summary?ccdc=1496223>.

### Crystallographic Experimental Details of **17a**·CHCl<sub>3</sub>

X-ray quality crystals of **17a**·CHCl<sub>3</sub> (C<sub>40</sub>H<sub>43</sub>N<sub>3</sub>OCu·CHCl<sub>3</sub>) were suspended in mineral oil at ambient temperature and a suitable crystal was selected. A mineral oil coated purple needle thereby obtained of approximate dimensions 0.030 mm x 0.050 mm x 0.190 mm was mounted on a 50  $\mu\text{m}$  MicroMesh MiTeGen Micromount and transferred to a Bruker AXS SMART APEX CCD X-ray diffractometer. The X-ray diffraction data were collected at 100(2) K using Mo-K $\alpha$  ( $\lambda = 0.71073 \text{ \AA}$ ) radiation. A total of 3672 frames were collected. The total exposure time was 20.4 hours. The frames were integrated with the Bruker SAINT software package using a narrow-frame algorithm.<sup>S1</sup> The integration of the data using a triclinic unit cell yielded a total of 62212 reflections to a maximum  $\theta$  angle of  $28.70^\circ$  ( $0.74 \text{ \AA}$  resolution), of which 9286 were independent (average redundancy 6.700, completeness = 99.1%,  $R_{int} = 4.72\%$ ,  $R_{sig} = 3.18\%$ ) and 7645 (82.33%) were observed with  $F_o^2 > 2\sigma(F_o^2)$ . The final cell constants of  $a = 12.6923(7) \text{ \AA}$ ,  $b = 13.2018(7) \text{ \AA}$ ,  $c = 13.6120(8) \text{ \AA}$ ,  $\alpha = 64.986(3)^\circ$ ,  $\beta = 62.582(3)^\circ$ ,  $\gamma = 86.745(3)^\circ$ , volume =  $1807.56(18) \text{ \AA}^3$ , are based upon the refinement of the XYZ-centroids of 9892 reflections above  $20 \sigma(I)$  with  $4.589^\circ < 2\theta < 56.08^\circ$ . Limiting indices were as follows:  $-17 \leq h \leq 17$ ,  $-17 \leq k \leq 17$ ,  $-18 \leq l \leq 18$ . Data were corrected for absorption effects using the multi-scan method (SADABS).<sup>S1</sup> The ratio of minimum to maximum apparent transmission was 0.931 with minimum and maximum SADABS generated transmission coefficients of 0.6939 and 0.7457. Solution and data analysis were performed using the WinGX software package.<sup>S2</sup> The structure was solved and refined in the space group  $P-1$  (no. 2) with  $Z = 2$ .<sup>S3</sup> The solution was achieved by charge-flipping methods using the program SUPERFLIP<sup>S4</sup> and the refinement was completed using the program SHELXL-2014/7.<sup>S5</sup> All non-H atoms were refined anisotropically. All H atoms were included in the refinement in the riding-model approximation (C--H = 0.95, 0.98, 0.99, and 1.00  $\text{\AA}$  for Ar--H, CH<sub>3</sub>, CH<sub>2</sub> and CH;  $U_{iso}(\text{H}) = 1.2U_{eq}(\text{C})$  except for methyl groups, where  $U_{iso}(\text{H}) = 1.5U_{eq}(\text{C})$ ). Full-matrix least-squares refinement on  $F^2$  led to convergence,  $(\Delta/\sigma)_{max} = 0.001$ ,  $(\Delta/\sigma)_{mean} = 0.000$ , with  $R_I = 0.0338$  and

$wR_2 = 0.0824$  for 7645 data with  $F_o^2 > 2\sigma(F_o^2)$  using 0 restraints and 444 parameters. A final difference Fourier synthesis showed features in the range of  $\Delta\rho_{max} = 0.646 \text{ e}/\text{\AA}^3$  to  $\Delta\rho_{min} = -0.500 \text{ e}/\text{\AA}^3$ . All residual electron density was within accepted norms and was deemed of no chemical significance. Molecular diagrams were generated using WinGX.<sup>S2</sup> CCDC-1496224 contains the supplementary crystallographic data for this structure. These data can be obtained free of charge from the Cambridge Crystallographic Data Centre via <https://summary.ccdc.cam.ac.uk/structure-summary?ccdc=1496224>.

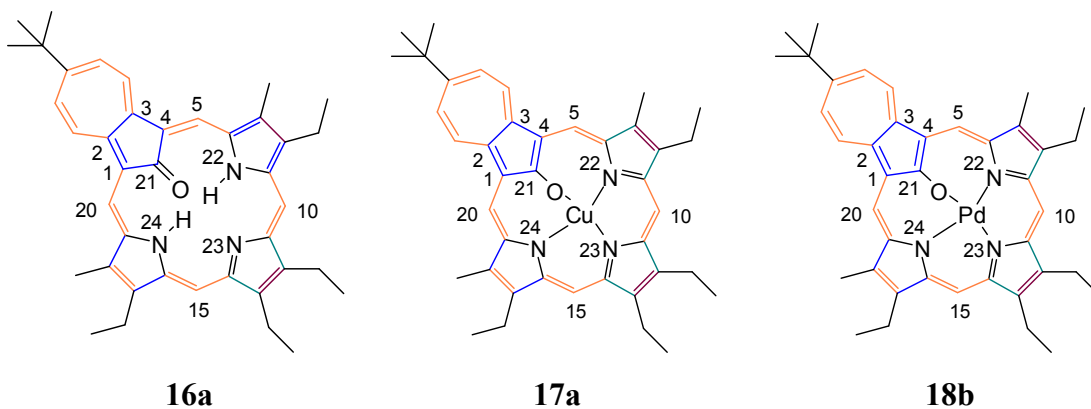
### Crystallographic Experimental Details of 18b

X-ray quality crystals of **18b** ( $\text{C}_{40}\text{H}_{43}\text{N}_3\text{OPd}$ ) were suspended in mineral oil at ambient temperature and a suitable crystal was selected. A mineral oil coated dark green plate thereby obtained of approximate dimensions 0.015 mm x 0.075 mm x 0.200 mm was mounted on a 50  $\mu\text{m}$  MicroMesh MiTeGen Micromount and transferred to a Bruker AXS SMART APEX CCD X-ray diffractometer. The X-ray diffraction data were collected at 100(2) K using Mo- $K_\alpha$  ( $\lambda = 0.71073 \text{ \AA}$ ) radiation. A total of 3672 frames were collected. The total exposure time was 30.60 hours. The frames were integrated with the Bruker SAINT software package using a narrow-frame algorithm.<sup>S1</sup> The integration of the data yielded a total of 64514 reflections to a maximum  $\theta$  angle of  $32.34^\circ$  (0.66  $\text{\AA}$  resolution), of which 10801 were independent (average redundancy 5.973, completeness = 94.6%,  $R_{\text{int}} = 4.47\%$ ,  $R_{\text{sig}} = 3.67\%$ ) and 8910 (82.49%) were observed with  $F_o^2 > 2\sigma(F_o^2)$ . The final triclinic cell constants of  $a = 11.5534(7) \text{ \AA}$ ,  $b = 12.8890(8) \text{ \AA}$ ,  $c = 13.1228(8) \text{ \AA}$ ,  $\alpha = 94.893(4)^\circ$ ,  $\beta = 114.886(3)^\circ$ ,  $\gamma = 110.418(3)^\circ$ , volume =  $1598.20(18) \text{ \AA}^3$ , are based upon the refinement of the XYZ-centroids of 9883 reflections above  $20 \sigma(I)$  with  $4.757^\circ < 2\theta < 58.20^\circ$ . Limiting indices were as follows:  $-17 \leq h \leq 16$ ,  $-18 \leq k \leq 18$ ,  $-19 \leq l \leq 19$ . Data were corrected for absorption effects using the multi-scan method (SADABS).<sup>S1</sup> The ratio of minimum to maximum apparent transmission was 0.941 with minimum and maximum SADABS generated transmission coefficients of 0.7000 and 0.7436. Solution and data analysis were performed using the WinGX software package.<sup>S2</sup> The structure was solved and refined in the space group  $P-1$  (no. 2) with  $Z = 2$ .<sup>S3</sup> The solution was achieved by charge-flipping methods using the program SUPERFLIP<sup>S4</sup> and the refinement was completed using the program SHELXL-2014/7.<sup>S5</sup> All non-H atoms were refined anisotropically. Twenty-three of the non-hydrogen atoms displayed a two PART positional disorder, which modeled best with a free variable which converged to 0.55721. All H

atoms were included in the refinement in the riding-model approximation (C--H = 0.95, 0.98, and 0.99 Å for Ar--H, CH<sub>3</sub>, and CH<sub>2</sub>;  $U_{\text{iso}}(\text{H}) = 1.2U_{\text{eq}}(\text{C})$  except for methyl groups, where  $U_{\text{iso}}(\text{H}) = 1.5U_{\text{eq}}(\text{C})$ ). Full-matrix least-squares refinement on  $F^2$  led to convergence,  $(\Delta/\sigma)_{\text{max}} = 0.001$ ,  $(\Delta/\sigma)_{\text{mean}} = 0.000$ , with  $R_1 = 0.0380$  and  $wR_2 = 0.0957$  for 8910 data with  $F_o^2 > 2\sigma(F_o^2)$  using 39 restraints and 618 parameters. A final difference Fourier synthesis showed features in the range of  $\Delta\rho_{\text{max}} = 1.863 \text{ e}/\text{\AA}^3$  to  $\Delta\rho_{\text{min}} = -1.526 \text{ e}/\text{\AA}^3$ . All residual electron density was within accepted norms and was deemed of no chemical significance, with the largest peaks being near the metal center. Molecular diagrams were generated using WinGX.<sup>S2</sup> CCDC-1496225 contains the supplementary crystallographic data for this structure. These data can be obtained free of charge from the Cambridge Crystallographic Data Centre via <https://summary.ccdc.cam.ac.uk/structure-summary?ccdc=1496225>.

## References

- S1 Bruker, *APEX2*, Bruker AXS Inc., Madison, Wisconsin, USA, 2014.
- S2 L. J. Farrugia, *J. Appl. Cryst.*, 2012, **45**, 849-854.
- S3 P. McArdle, *J. Appl. Cryst.*, 1996, **29**, 306.
- S4 L. Palatinus and G. Chapuis, *J. Appl. Cryst.* **2007**, *40*, 786-790.
- S5 G. M. Sheldrick, *Acta Cryst.*, 2015, **C71**, 3-8.
- S6 A. L. Spek, *Acta Cryst.*, 2015, **C71**, 9-18.

Table S1: Summary of framework bond distances (Å) and angles (°) for **16a**, **17a** and **18b**.

	<b>16a</b> (M = none)	<b>17a</b> (M = Cu)	<b>18b</b> (M = Pd)	<b>18b</b> (M = Pd)*
C21-O	1.270(3)	1.296(2)	1.298(2)	
M-O	--	1.9215(11)	1.9982(14)	
M-C21	--	2.551(2)	2.5114(19)	
M-N22	--	1.9981(13)	2.0123(18)	
M-N23	--	1.9054(14)	1.994(9)	1.972(13)
M-N24	--	1.9975(14)	2.0092(19)	
C2-C2a	1.400(4)	1.386(2)	1.390(3)	
C2a-C2b	1.383(4)	1.398(2)	1.395(3)	
C2b-C2c	1.410(4)	1.394(2)	1.401(3)	
C2c-C3b	1.393(4)	1.409(2)	1.403(3)	
C3b-C3a	1.394(4)	1.385(2)	1.387(3)	
C3a-C3	1.387(4)	1.397(2)	1.396(3)	
C21-C1	1.448(3)	1.423(2)	1.418(3)	
C1-C2	1.422(4)	1.435(2)	1.426(3)	
C2-C3	1.456(3)	1.459(2)	1.468(3)	
C3-C4	1.433(4)	1.425(2)	1.418(3)	
C4-C21	1.443(4)	1.428(2)	1.426(3)	
C4-C5	1.407(4)	1.413(2)	1.415(3)	
C5-C6	1.387(4)	1.380(2)	1.380(3)	
C6-N22	1.376(3)	1.404(2)	1.402(3)	
C6-C7	1.449(3)	1.459(2)	1.517(11)	1.412(16)
C7-C8	1.372(4)	1.356(2)	1.343(9)	1.347(11)
C8-C9	1.439(3)	1.455(2)	1.458(9)	1.467(11)
C9-N22	1.355(3)	1.360(2)	1.387(9)	1.355(15)
C9-C10	1.394(4)	1.403(2)	1.390(9)	1.398(11)
C10-C11	1.391(4)	1.378(2)	1.373(7)	1.370(9)
C11-N23	1.375(3)	1.371(2)	1.373(8)	1.373(10)
C11-C12	1.471(4)	1.458(2)	1.474(8)	1.476(10)
C12-C13	1.350(4)	1.359(2)	1.349(7)	1.347(9)
C13-C14	1.470(4)	1.459(2)	1.459(7)	1.465(10)
C14-N23	1.369(3)	1.372(2)	1.367(9)	1.375(12)

C14-C15	1.397(4)	1.379(2)	1.370(7)	1.348(9)
C15-C16	1.396(4)	1.407(2)	1.402(8)	1.399(10)
C16-N24	1.347(3)	1.365(2)	1.364(8)	1.399(10)
C16-C17	1.450(3)	1.450(2)	1.459(8)	1.445(11)
C17-C18	1.369(4)	1.357(2)	1.382(6)	1.373(9)
C18-C19	1.449(3)	1.454(2)	1.433(6)	1.497(9)
C19-N24	1.382(3)	1.401(2)	1.407(3)	
C19-C20	1.379(4)	1.382(2)	1.383(3)	
C20-C1	1.411(3)	1.404(2)	1.414(3)	
C21-O-M	--	103.23(10)	96.96(12)	
O-M-N22	--	88.85(5)	88.84(6)	
N22-M-N23	--	94.92(6)	88.0(2)	98.8(2)
N23-M-N24	--	93.88(6)	96.7(2)	86.2(3)
N24-M-O	--	88.35(5)	88.49(7)	
O-M-N23	--	153.03(5)	163.6(3)	159.9(3)
N22-M-N24	--	165.79(6)	171.85(7)	

\*Second PART of disordered atoms.

**Orange – more aromatic (1.38-1.41), green – single bond limit ( $\geq 1.46$ ), blue – more single bond like (1.42-1.45), purple more double bond like ( $\leq 1.37$ ).**

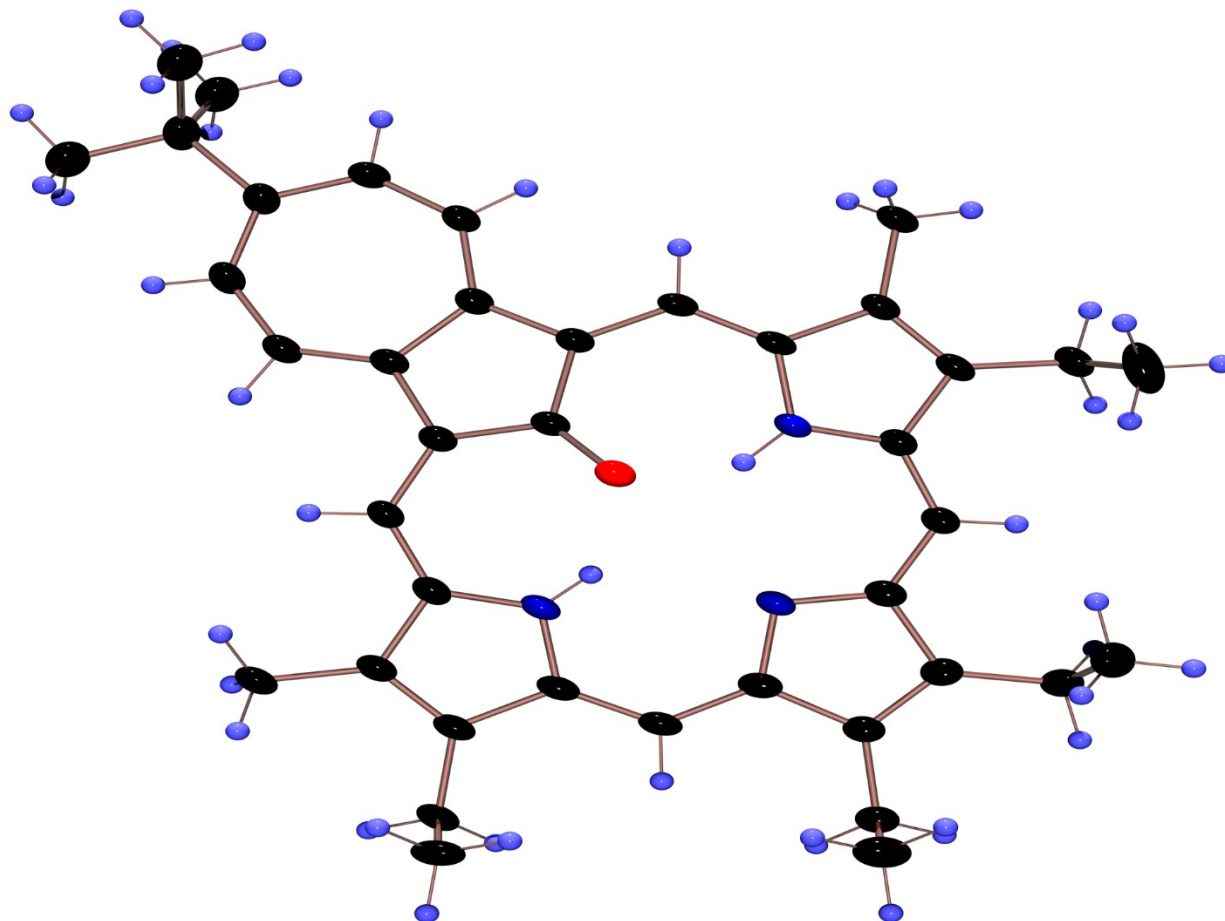


Figure S1. “Aerial-view”: Color POV-Ray rendered ORTEP III drawing (50% probability level, hydrogen atoms rendered arbitrarily small for clarity) of compound **16a**.

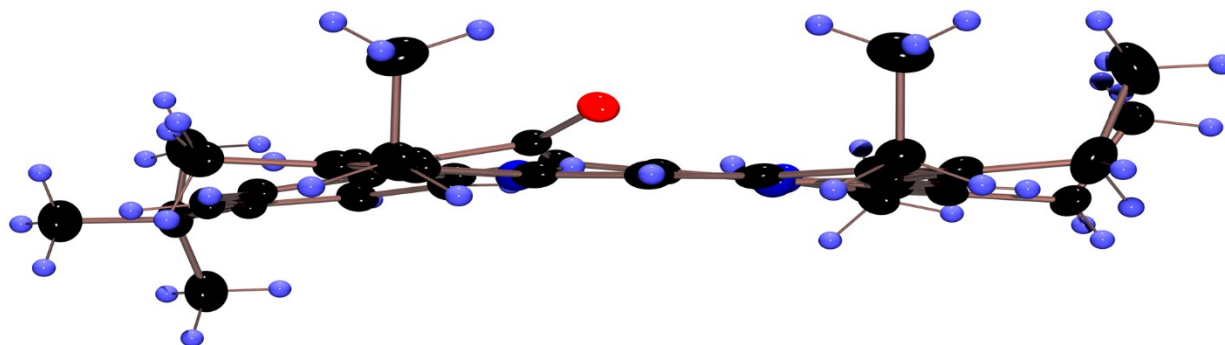


Figure S2. “Edge-view”: Color POV-Ray rendered ORTEP III drawing (50% probability level, hydrogen atoms rendered arbitrarily small for clarity) of compound **16a**.

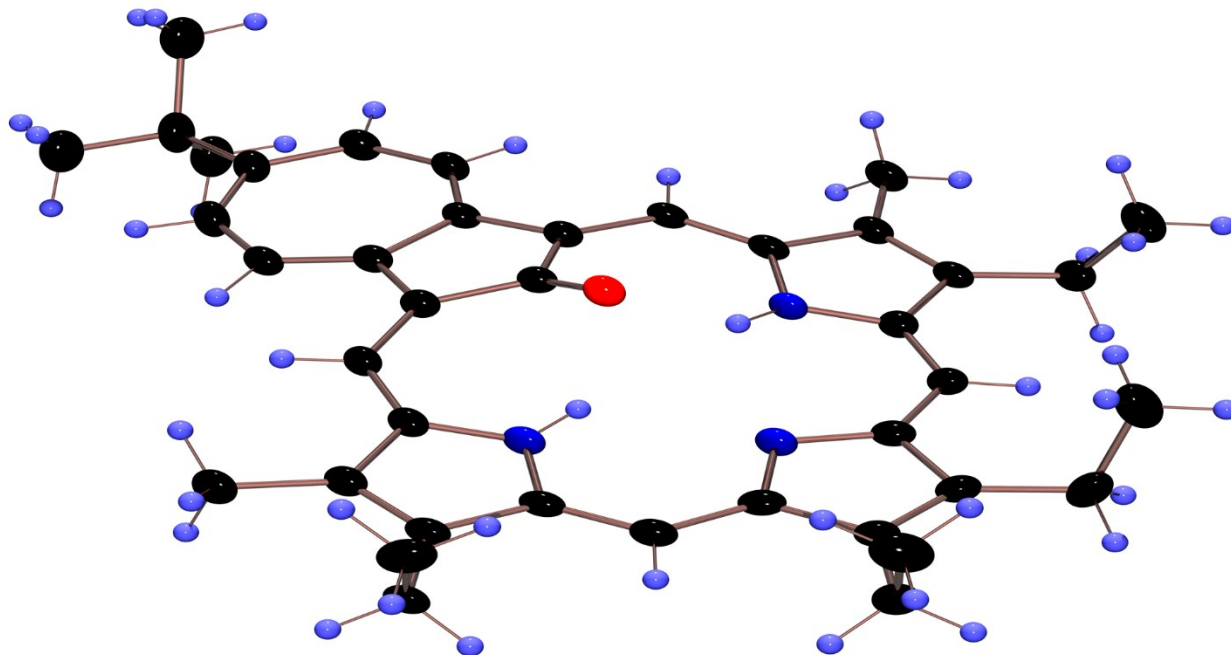


Figure S3. 45° from “edge-view”: Color POV-Ray rendered ORTEP III drawing (50% probability level, hydrogen atoms rendered arbitrarily small for clarity) of compound **16a**.

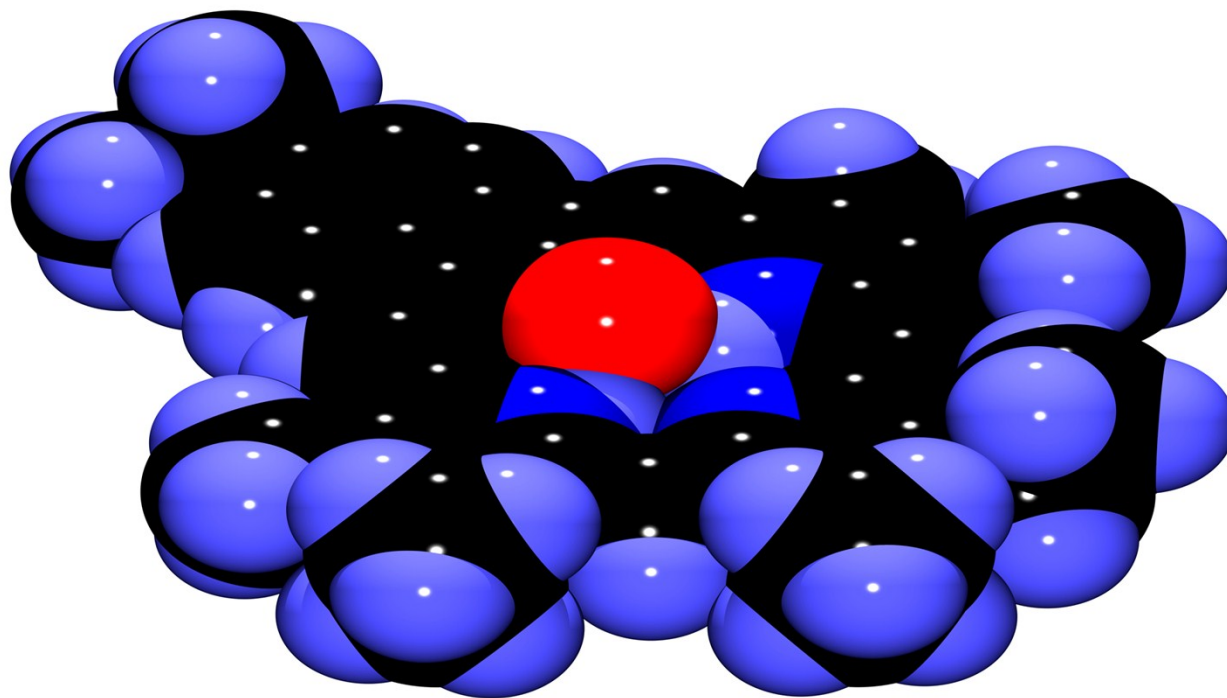


Figure S4. Color POV-Ray rendered space-filling drawing of compound **16a**.

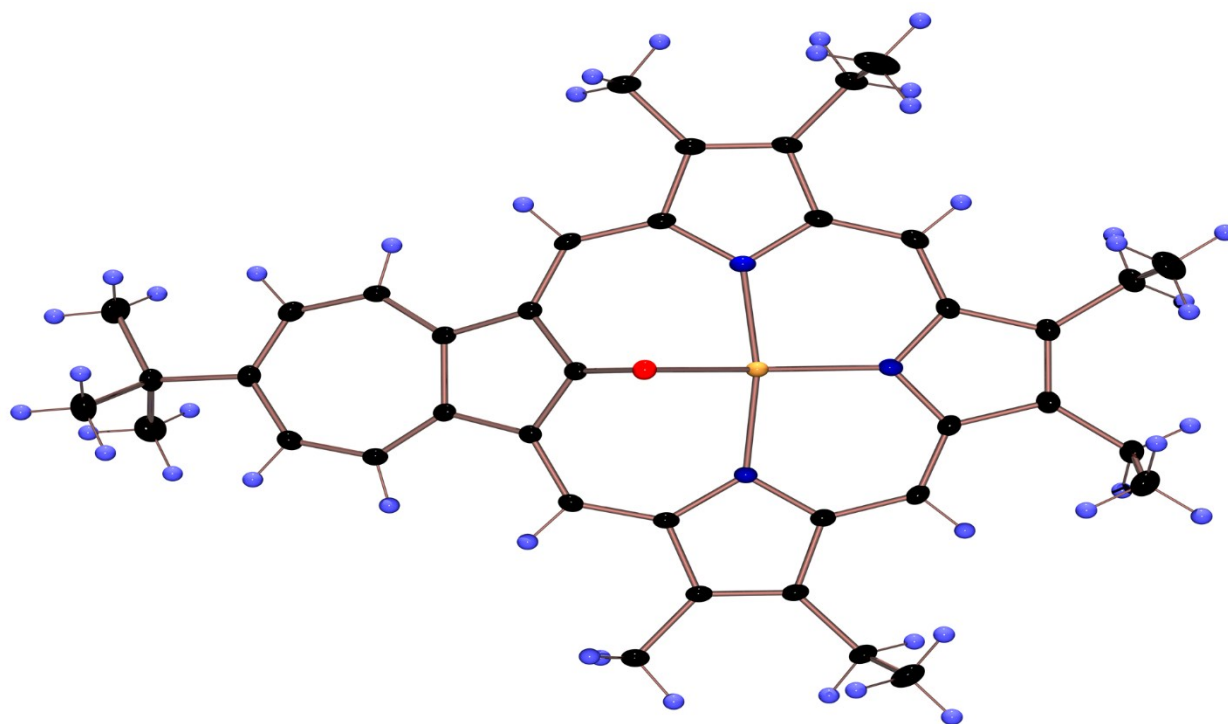


Figure S5. “Aerial-view”: Color POV-Ray rendered ORTEP III drawing (50% probability level, hydrogen atoms rendered arbitrarily small for clarity) of compound **17a**.

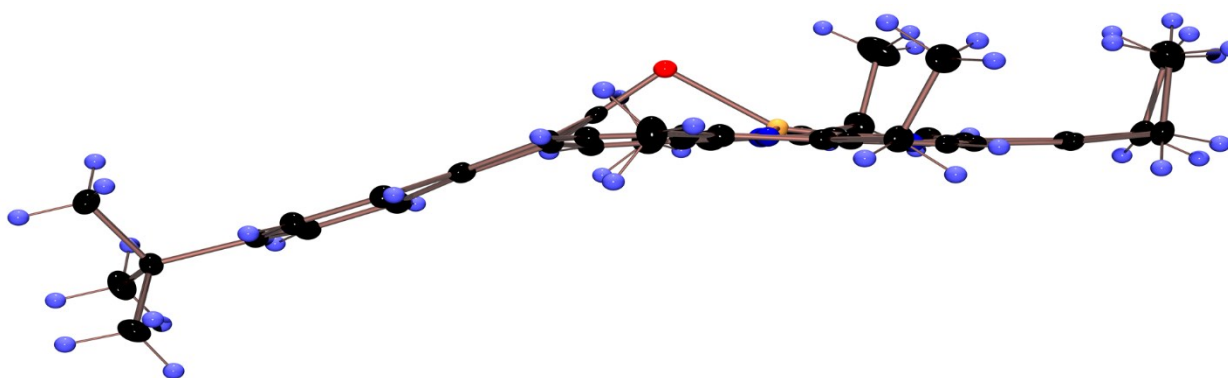


Figure S6. “Edge-view”: Color POV-Ray rendered ORTEP III drawing (50% probability level, hydrogen atoms rendered arbitrarily small for clarity) of compound **17a**.

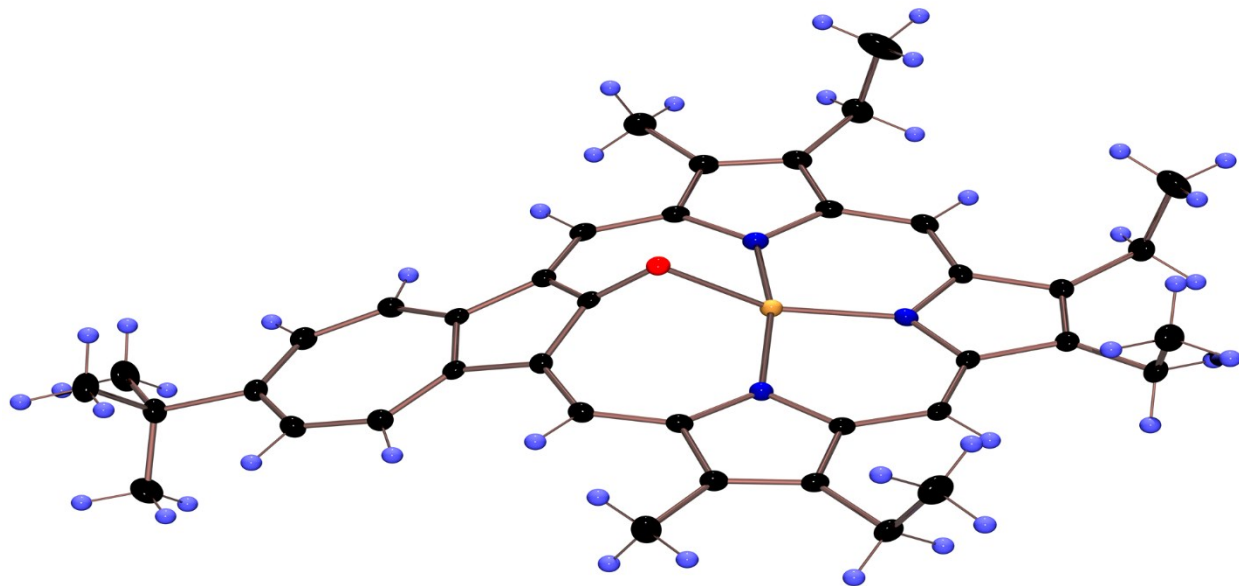


Figure S7. 45° from “edge-view”: Color POV-Ray rendered ORTEP III drawing (50% probability level, hydrogen atoms rendered arbitrarily small for clarity) of compound **17a**.

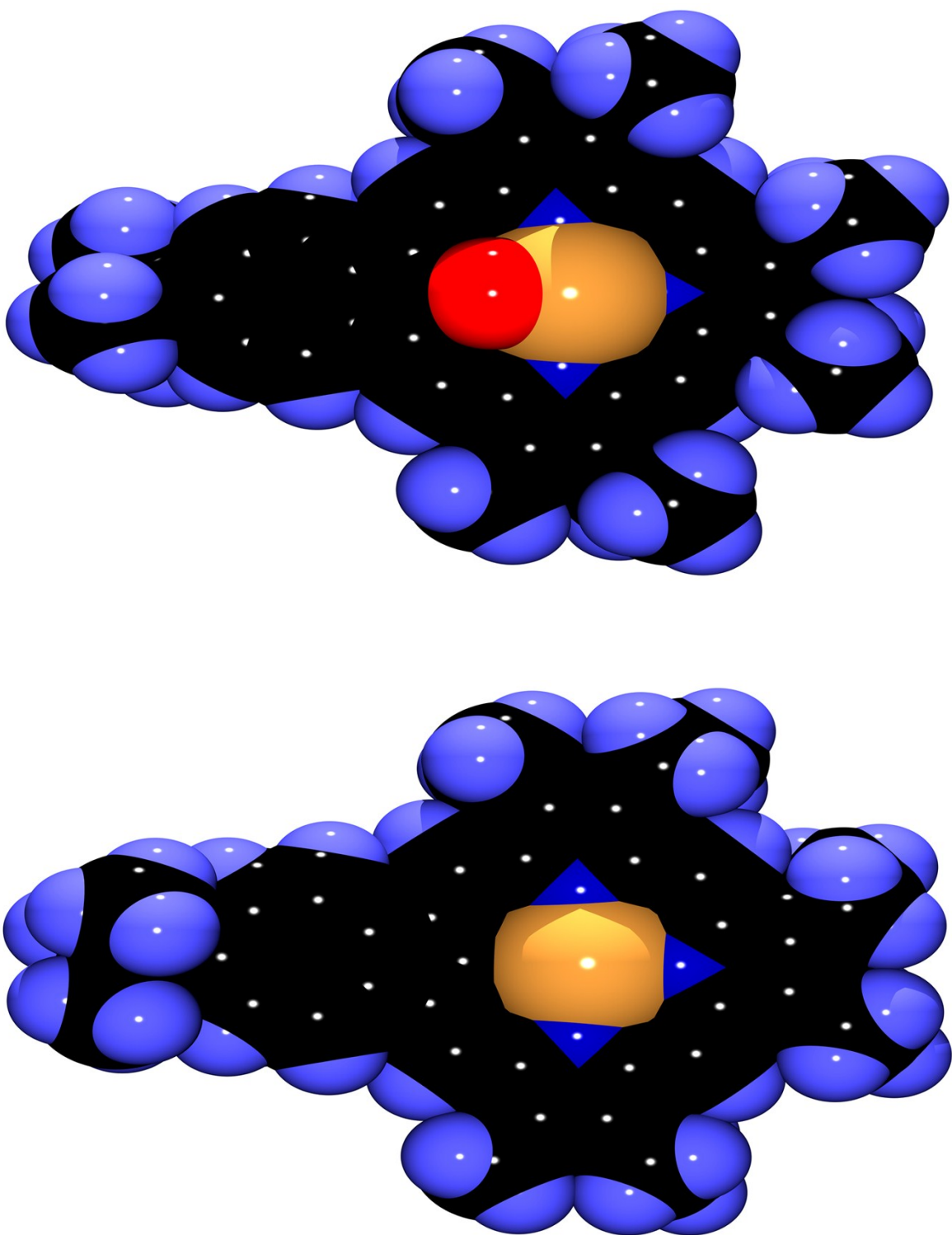


Figure S8. Color POV-Ray rendered space-filling drawings of compound **17a**.

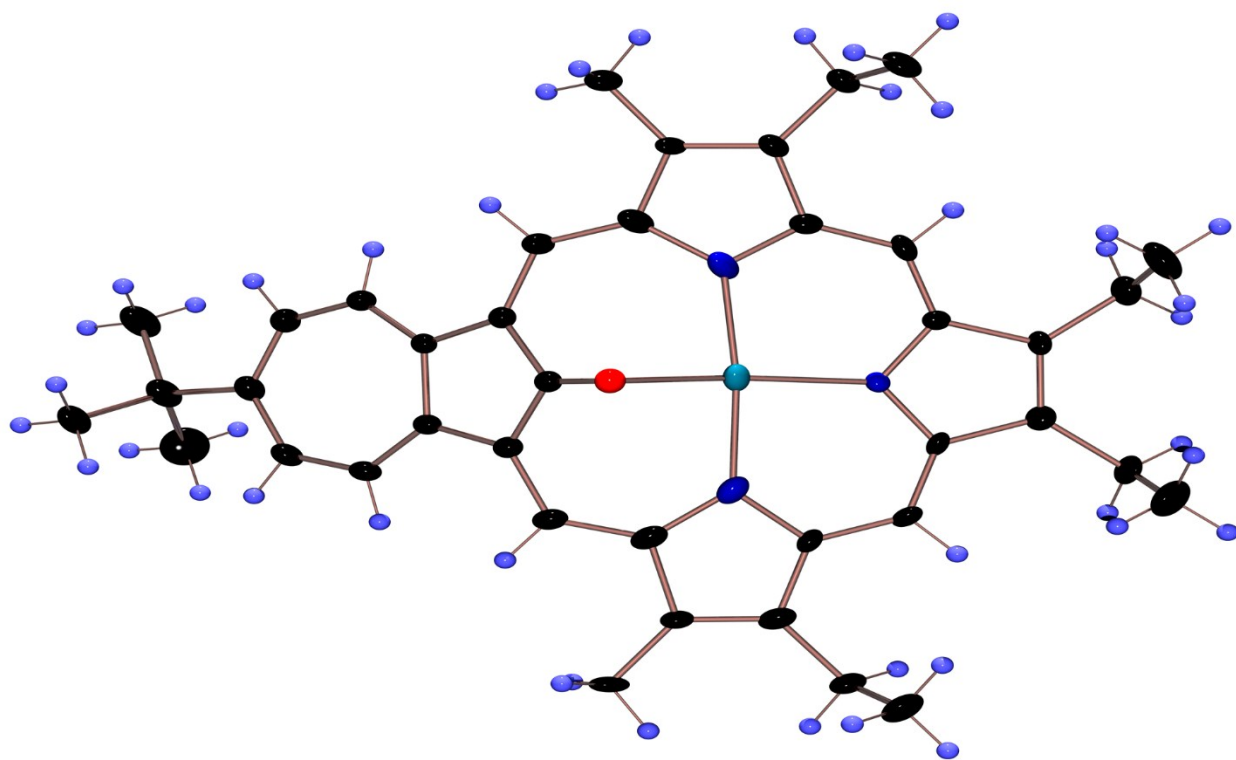


Figure S9. “Arial-view”: Color POV-Ray rendered ORTEP III drawing (50% probability level, hydrogen atoms rendered arbitrarily small for clarity) of compound **18b**.

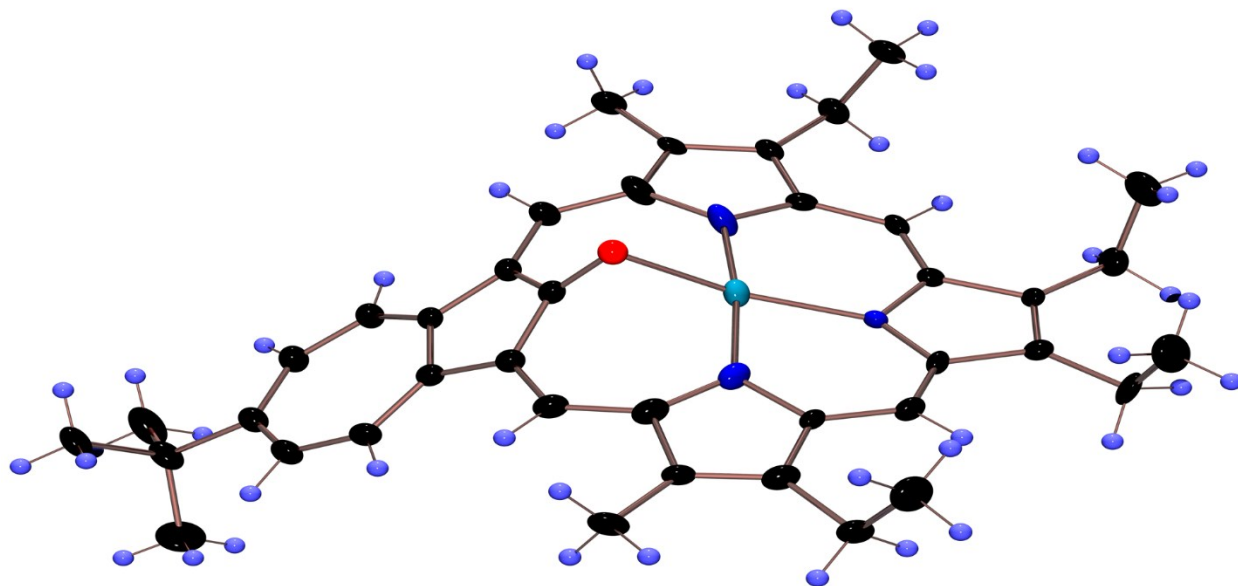


Figure S9. 45° from “edge-view”: Color POV-Ray rendered ORTEP III drawing (50% probability level, hydrogen atoms rendered arbitrarily small for clarity) of compound **18b**.

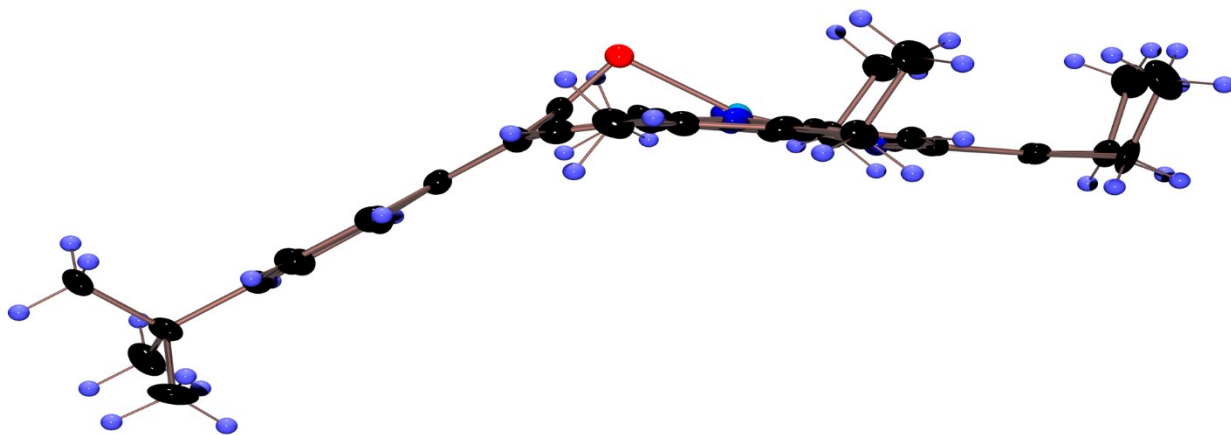


Figure S10. “Edge-view”: Color POV-Ray rendered ORTEP III drawing (50% probability level, hydrogen atoms rendered arbitrarily small for clarity) of compound **18b**.

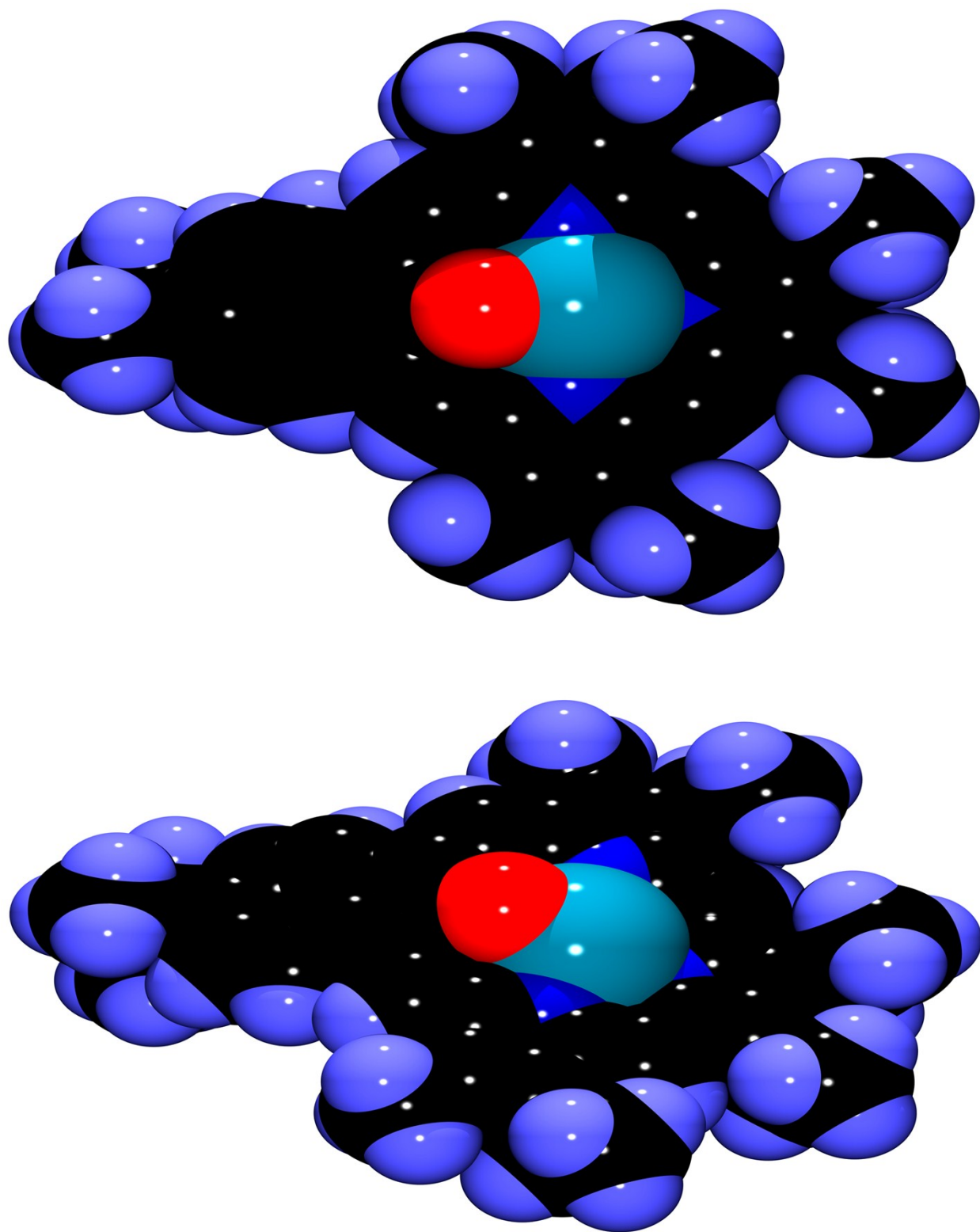


Figure S11. Color POV-Ray rendered space-filling drawings of compound **18b**.

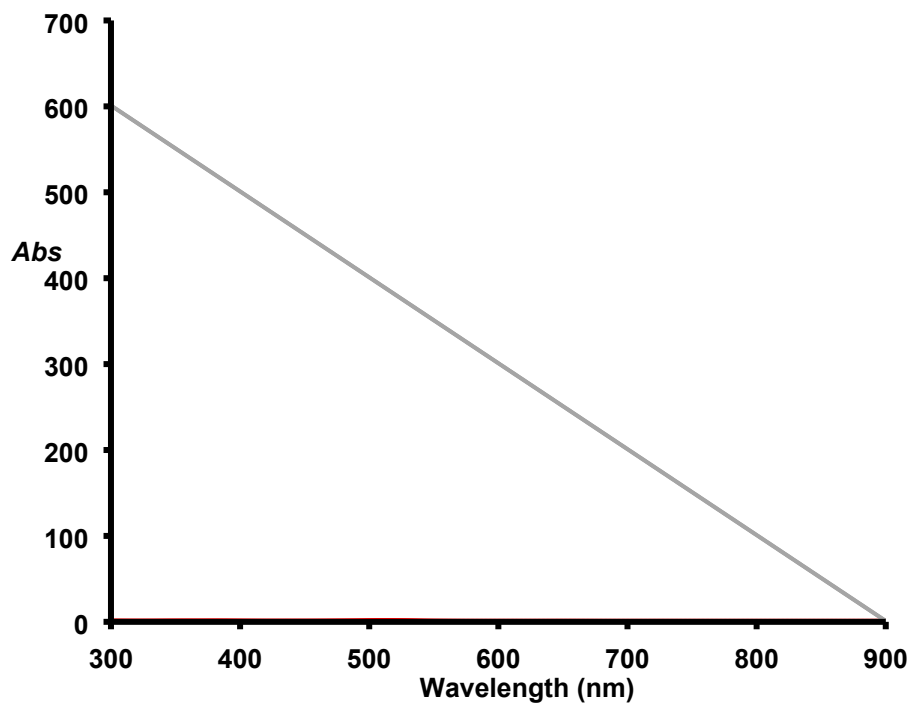


Figure S12. UV-vis spectrum of **16a** in 1% Et<sub>3</sub>N-CH<sub>2</sub>Cl<sub>2</sub>.

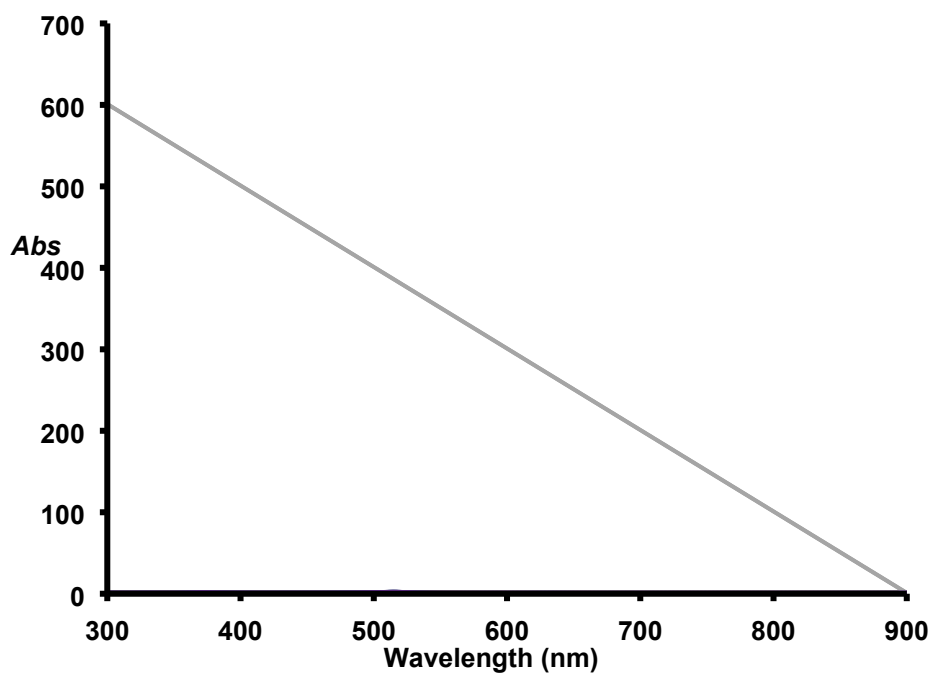


Figure S13. UV-vis spectra of **16a** in 1% Et<sub>3</sub>N-CH<sub>2</sub>Cl<sub>2</sub> (free base, red line), dichloromethane (green line) and with 1 equiv of TFA in CH<sub>2</sub>Cl<sub>2</sub> (purple line). Even though the dichloromethane had been deacidified, significant protonation occurred in CH<sub>2</sub>Cl<sub>2</sub>.

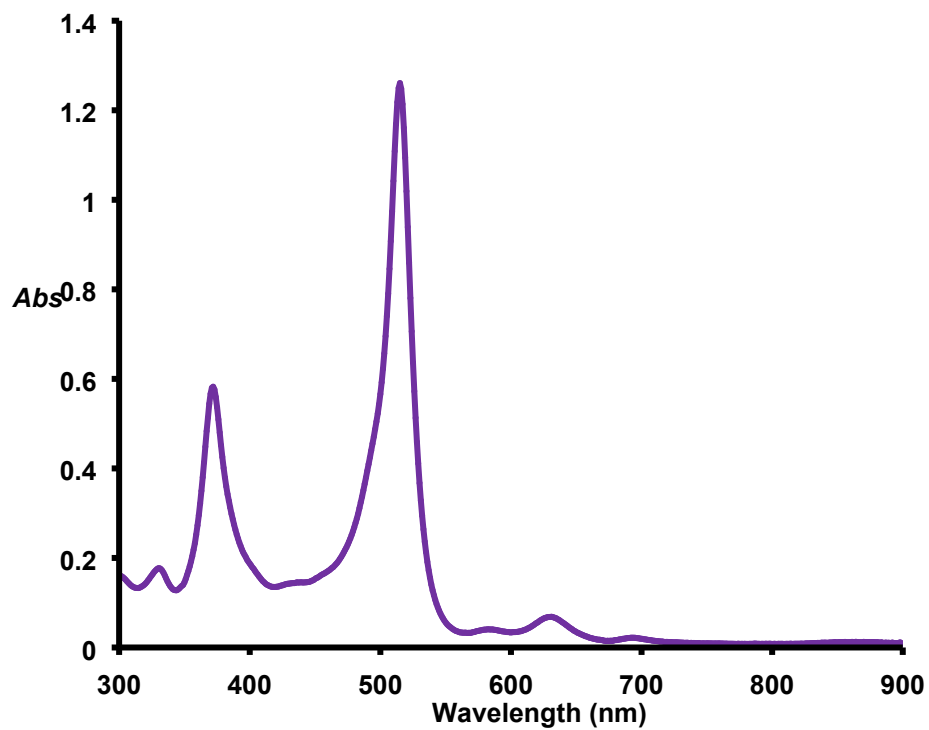


Figure S14. UV-vis spectrum of **16aH<sup>+</sup>** with 5 equiv of TFA in CH<sub>2</sub>Cl<sub>2</sub>.

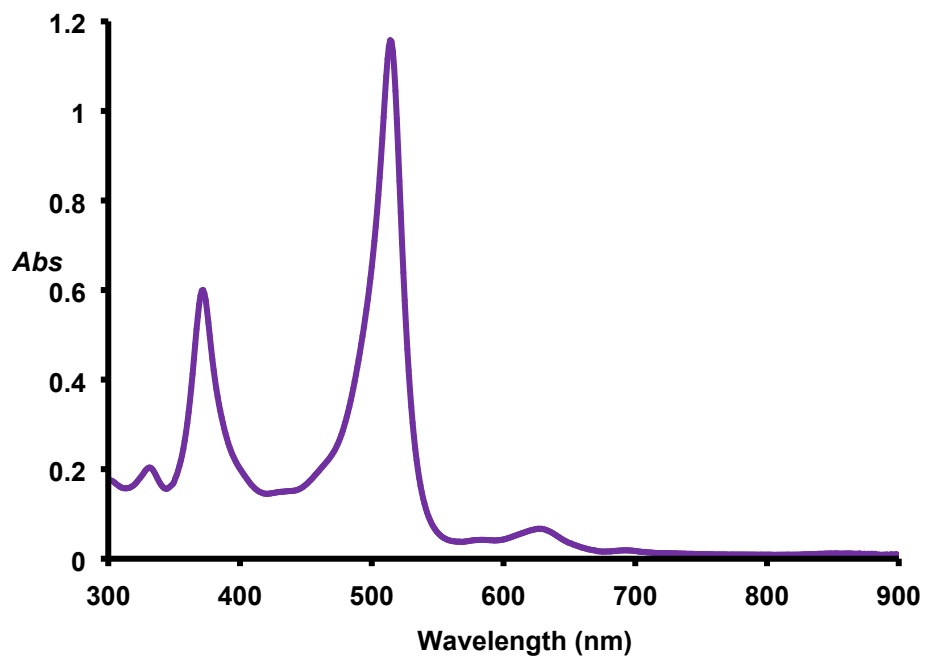


Figure S15. UV-vis spectrum of **16aH<sup>+</sup>** in 1% TFA-CH<sub>2</sub>Cl<sub>2</sub>.

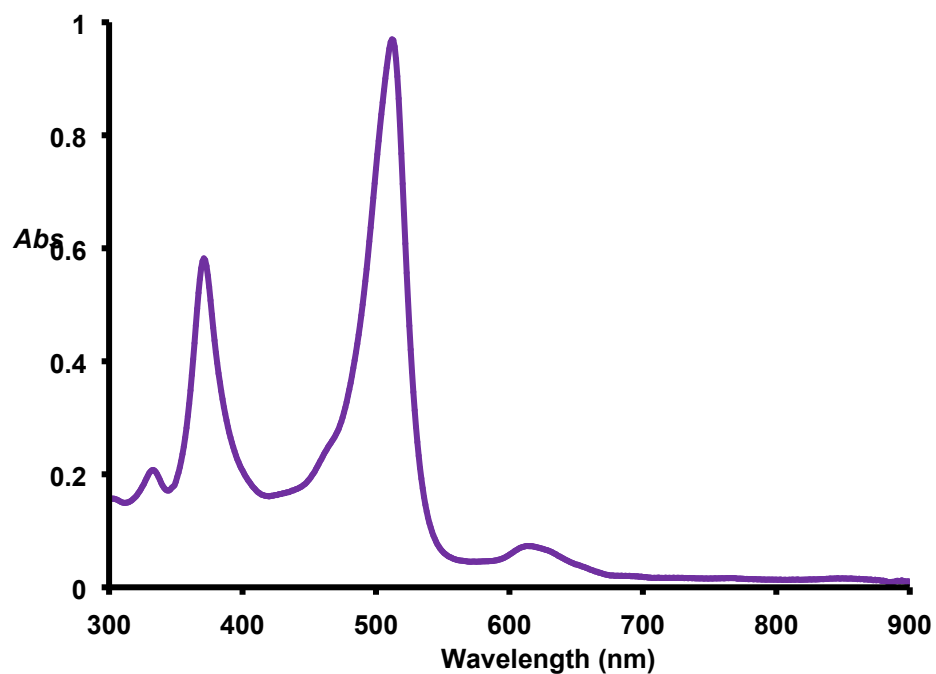


Figure S16. UV-vis spectrum of protonated oxyazuliporphyrin **16a** in 5% TFA-CH<sub>2</sub>Cl<sub>2</sub>.

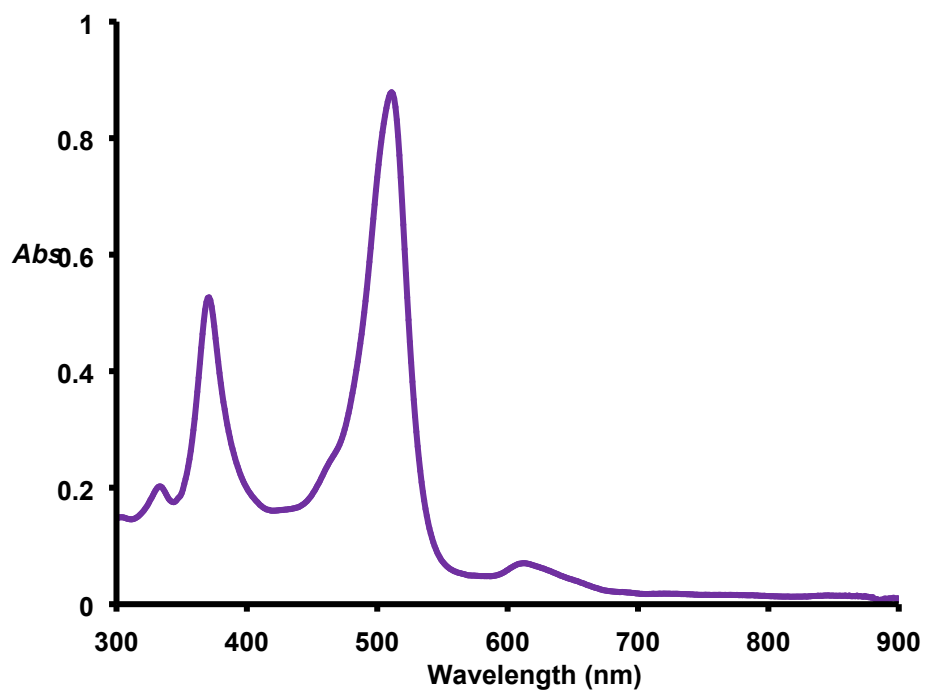


Figure S17. UV-vis spectrum of protonated oxyazuliporphyrin **16a** in 10% TFA-CH<sub>2</sub>Cl<sub>2</sub>.

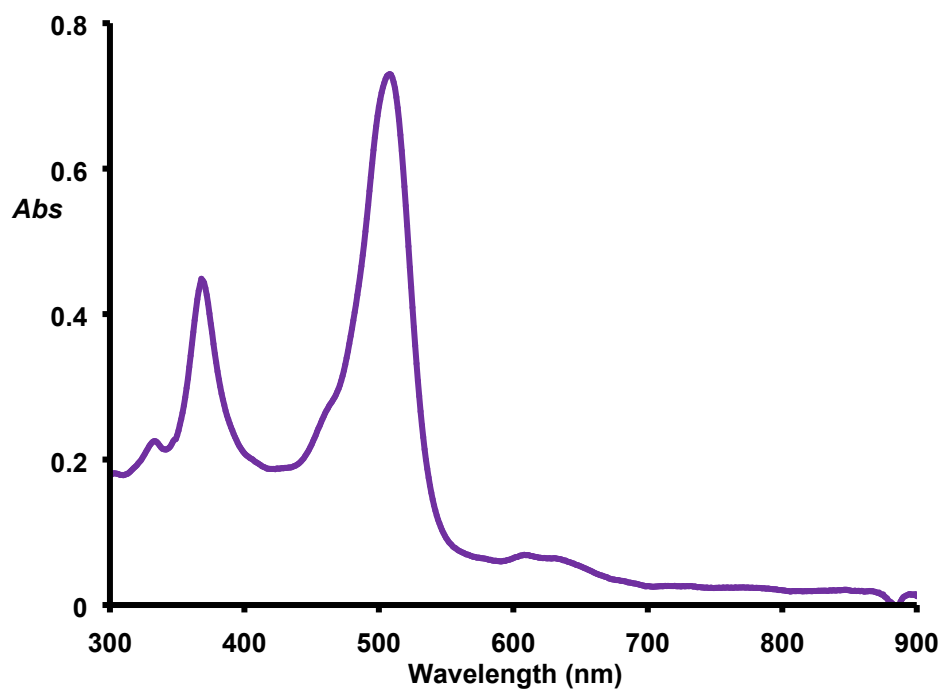


Figure S18. UV-vis spectrum of protonated oxyazuliporphyrin **16a** in 50% TFA-CH<sub>2</sub>Cl<sub>2</sub>.

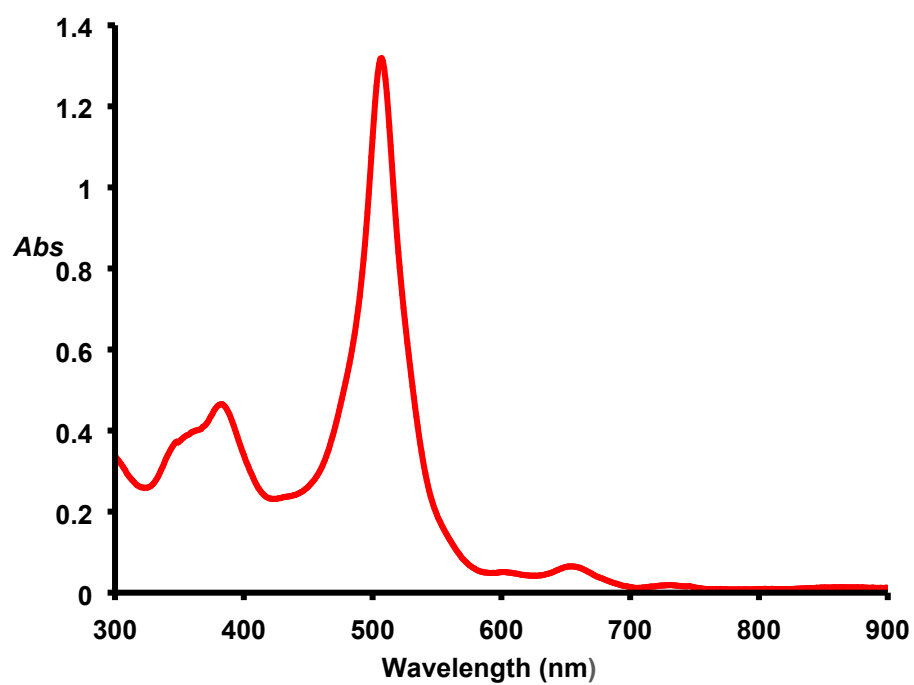


Figure S19. UV-vis spectrum of oxyazuliporphyrin **16b** in 1% Et<sub>3</sub>N-CH<sub>2</sub>Cl<sub>2</sub>.

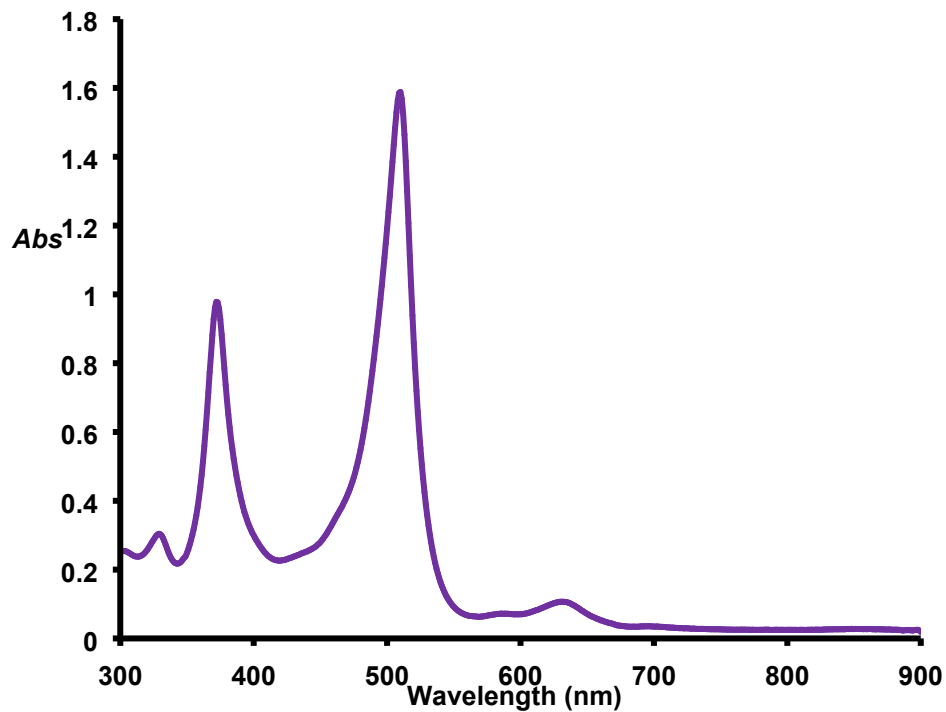


Figure S20. UV-vis spectrum of protonated oxyazuliporphyrin **16b** in 1% TFA-CH<sub>2</sub>Cl<sub>2</sub>.

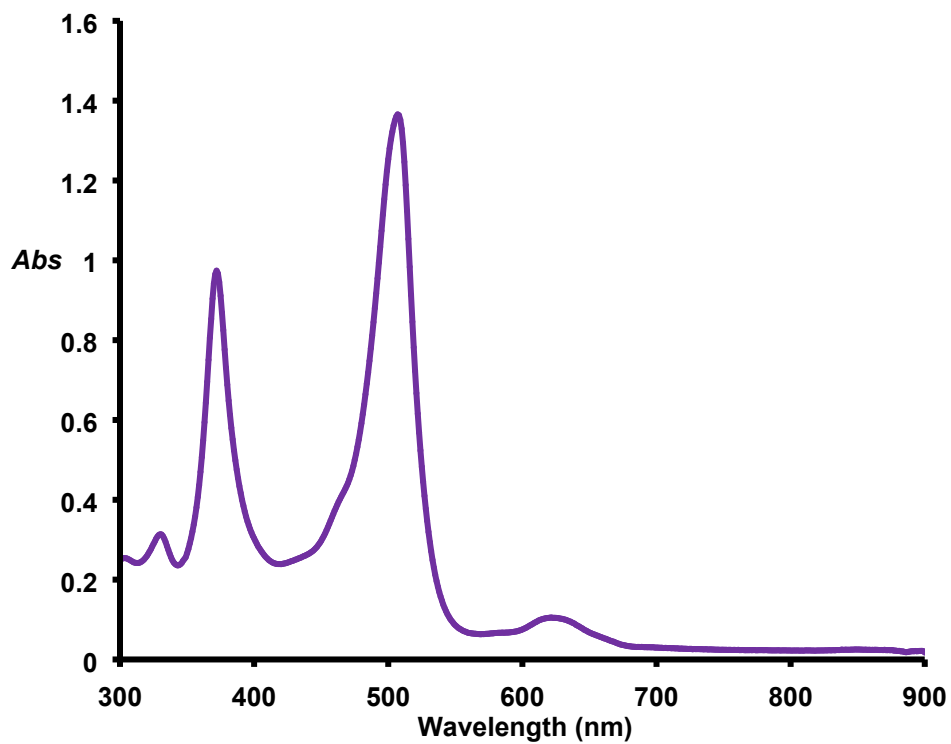


Figure S21. UV-vis spectrum of protonated oxyazuliporphyrin **16b** in 5% TFA-CH<sub>2</sub>Cl<sub>2</sub>.

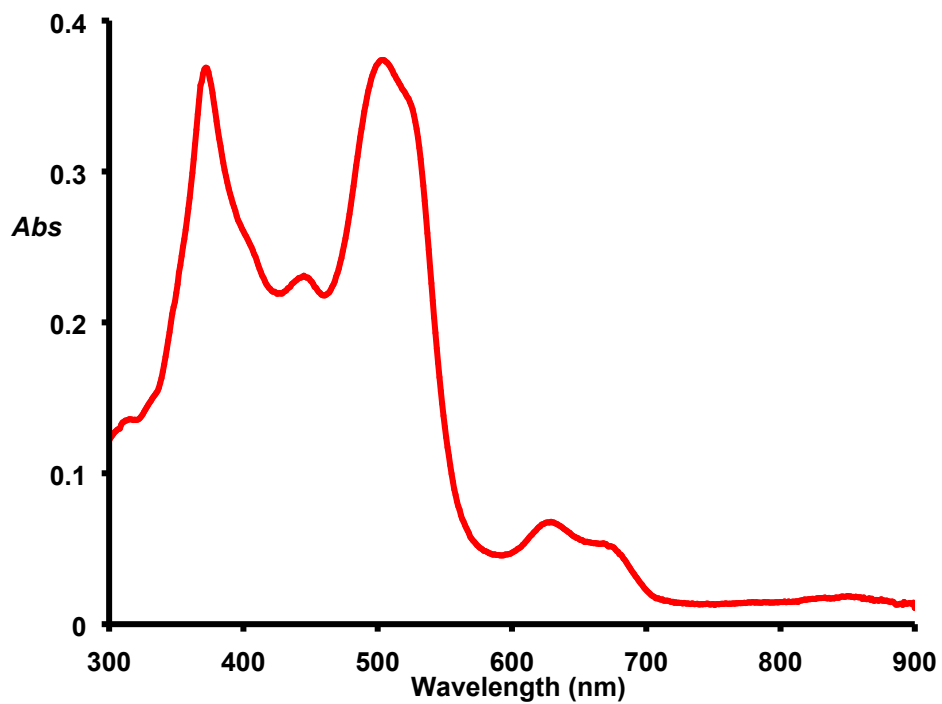


Figure S22. UV-vis spectrum of copper(II) oxyazuliporphyrin **17a** in  $\text{CH}_2\text{Cl}_2$ .

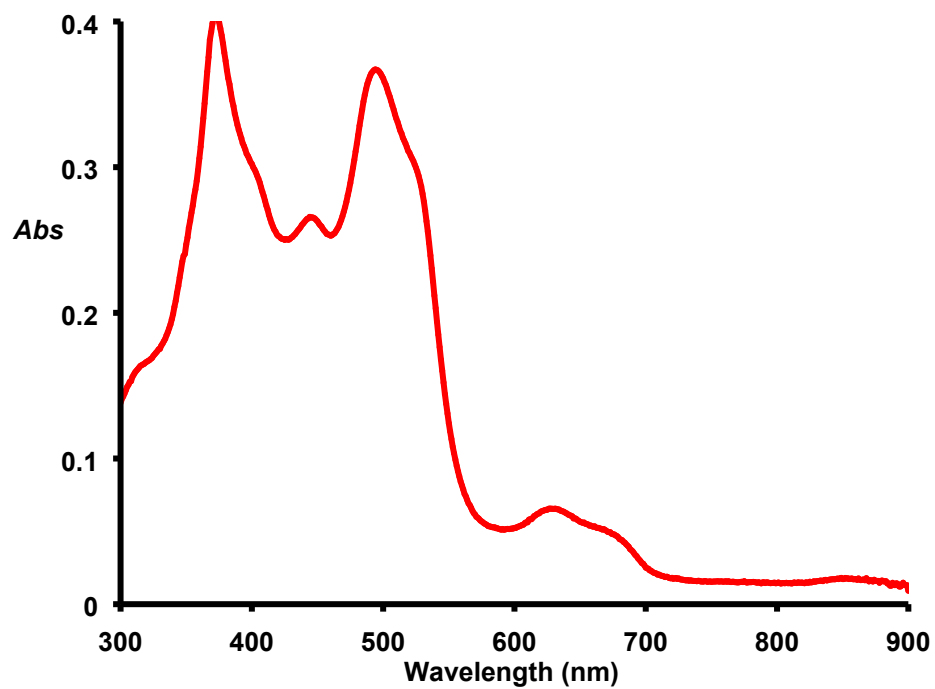


Figure S23. UV-vis spectrum of copper(II) oxyazuliporphyrin **17b** in  $\text{CH}_2\text{Cl}_2$ .

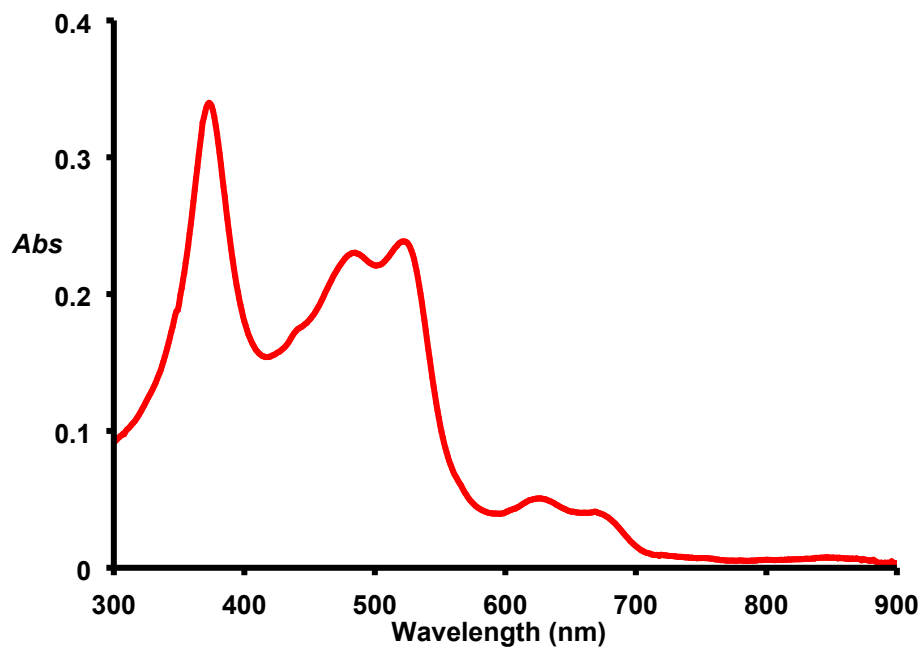


Figure S24. UV-vis spectrum of nickel(II) oxyazuliporphyrin **18a** in  $\text{CH}_2\text{Cl}_2$ .

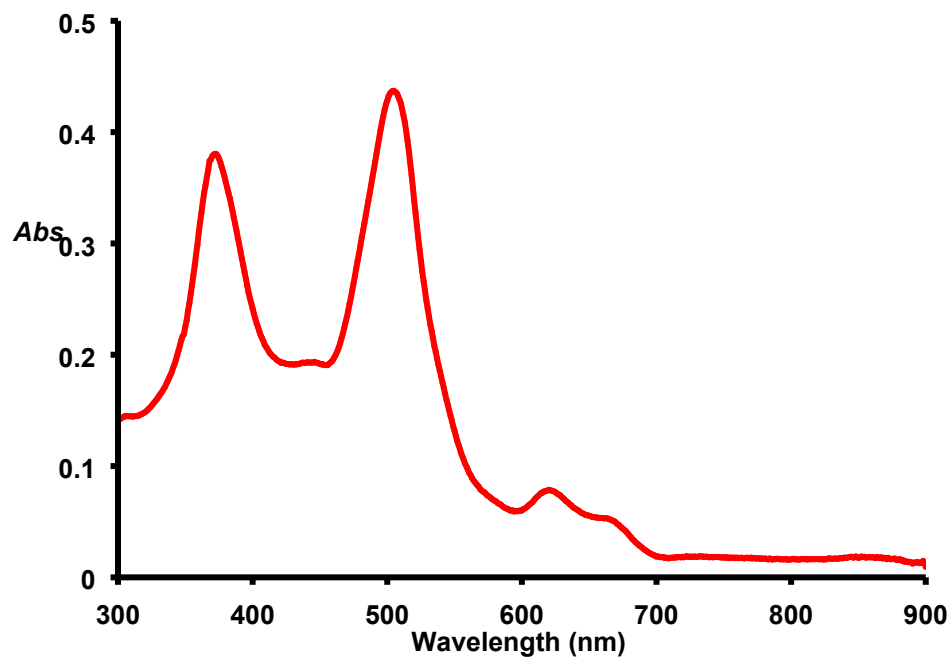


Figure S25. UV-vis spectrum of palladium(II) oxyazuliporphyrin **18b** in  $\text{CH}_2\text{Cl}_2$ .

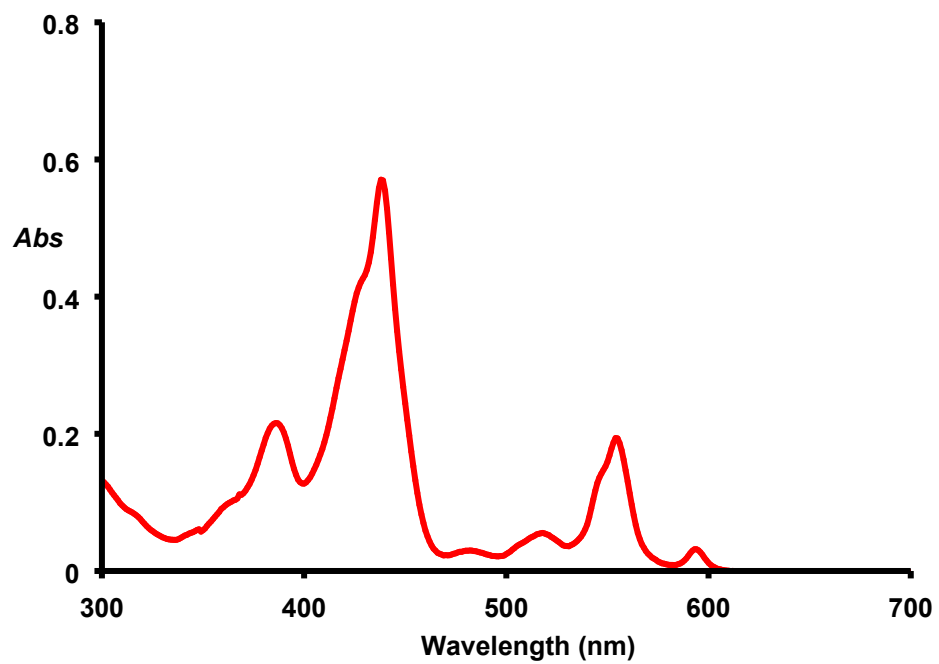


Figure S26. UV-vis spectrum of silver(III) benzocarbaporphyrin **21a** in  $\text{CH}_2\text{Cl}_2$ .

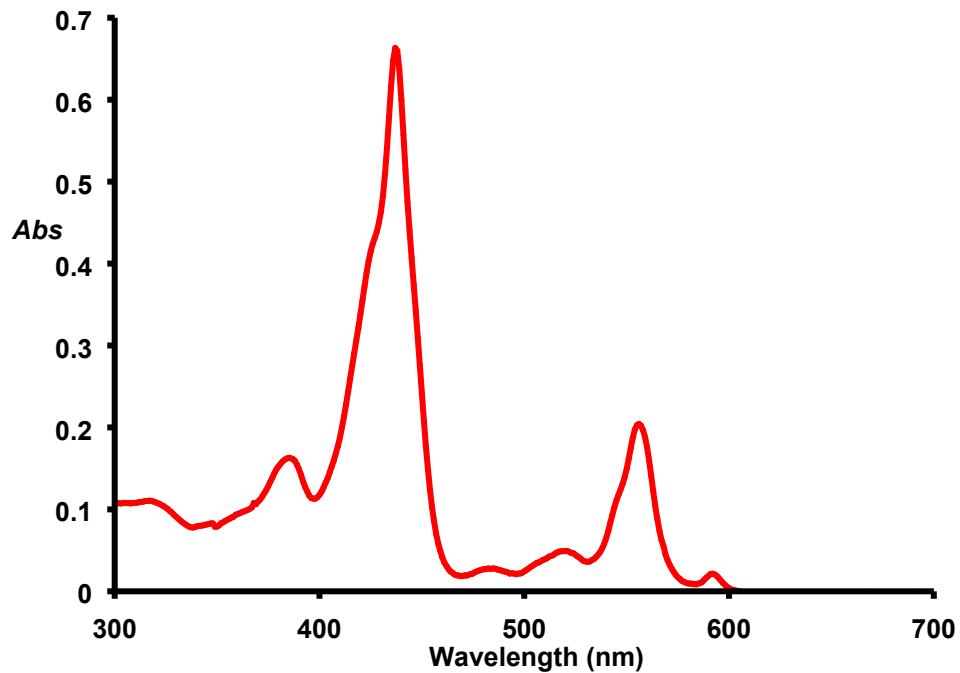


Figure S27. UV-vis spectrum of silver(III) benzocarbaporphyrin **21b** in  $\text{CH}_2\text{Cl}_2$ .

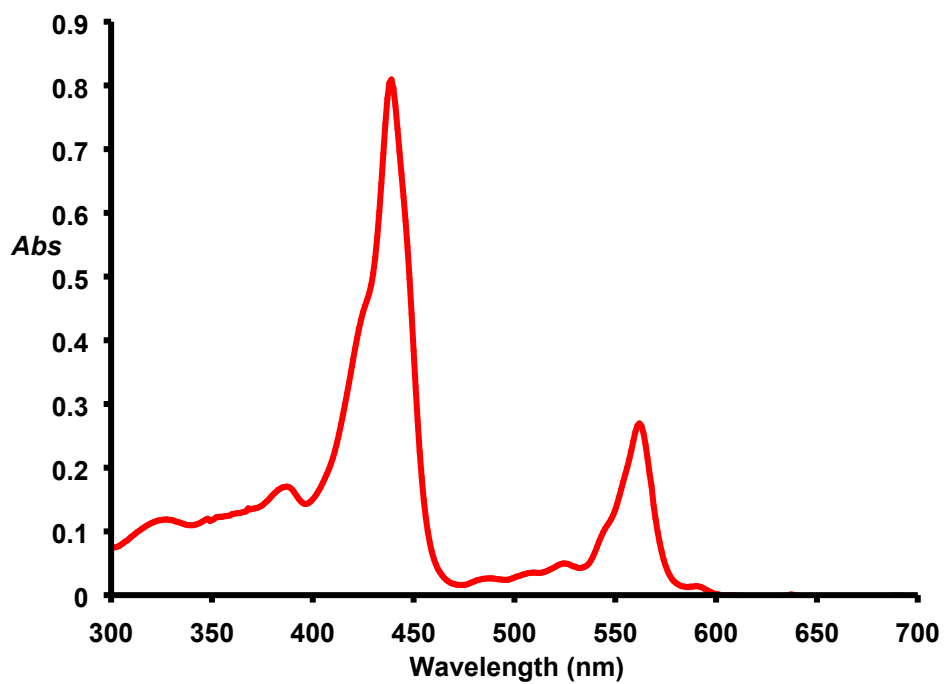


Figure S28. UV-vis spectrum of silver(III) benzocarbaporphyrin **22c** in  $\text{CH}_2\text{Cl}_2$ .

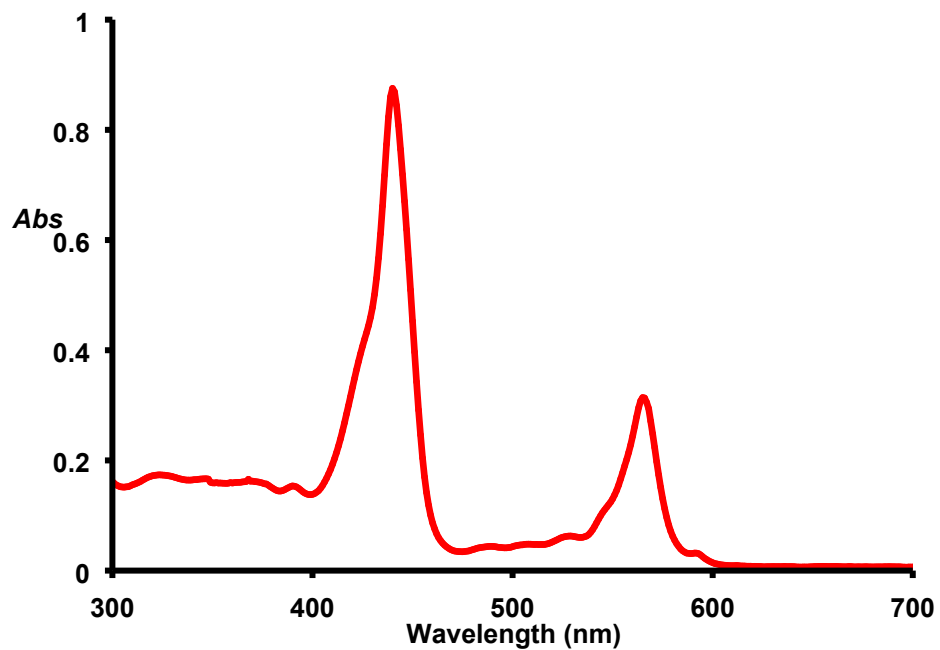


Figure S29. UV-vis spectrum of silver(III) benzocarbaporphyrin **22b** in  $\text{CH}_2\text{Cl}_2$ .

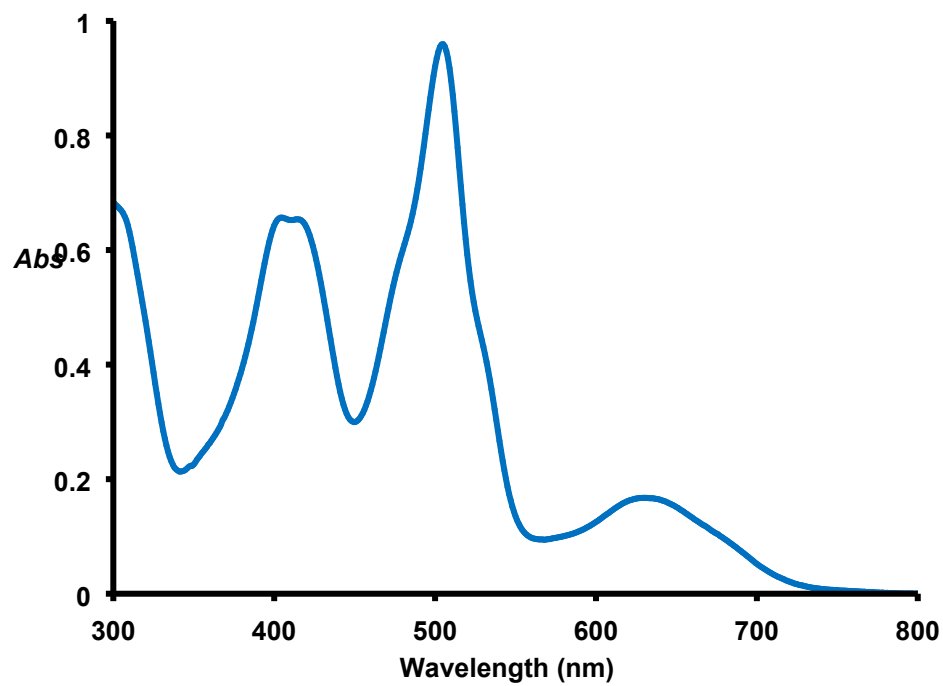


Figure S30. UV-vis spectrum of palladium(III) thiocarbaporphyrin **29a** in  $\text{CH}_2\text{Cl}_2$ .

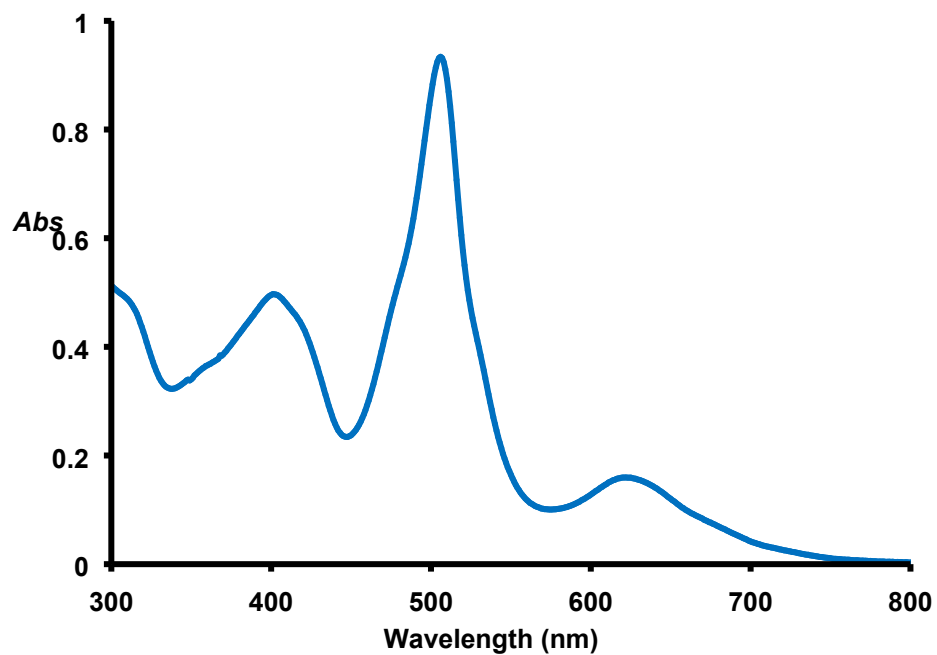


Figure S31. UV-vis spectrum of palladium(III) thiocarbaporphyrin **29b** in  $\text{CH}_2\text{Cl}_2$ .

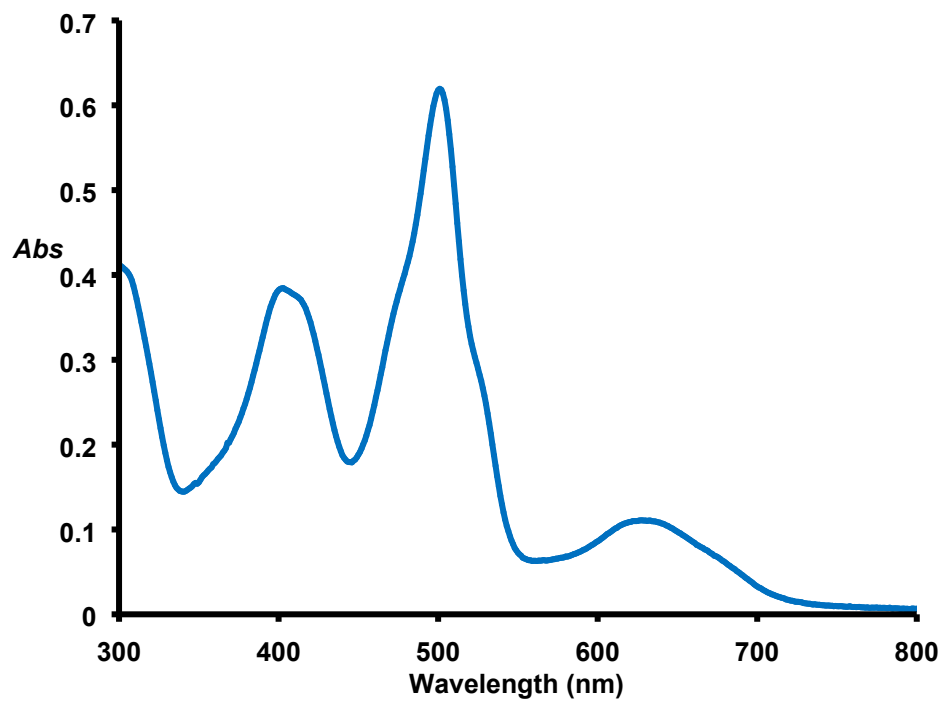


Figure S32. UV-vis spectrum of palladium(III) thiocarbaporphyrin **29c** in  $\text{CH}_2\text{Cl}_2$ .

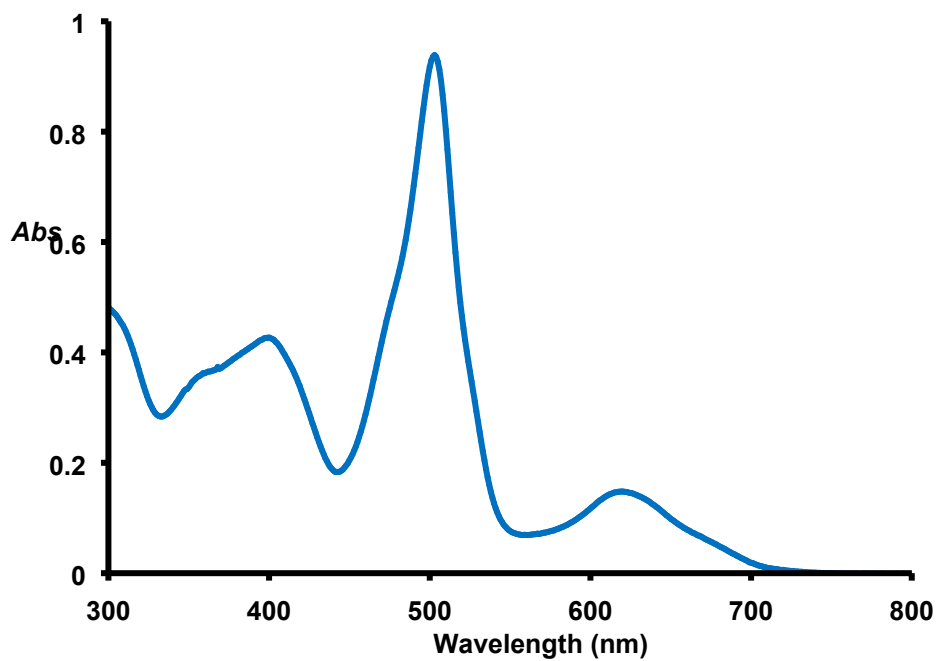


Figure S33. UV-vis spectrum of palladium(III) thiocarbaporphyrin **29d** in  $\text{CH}_2\text{Cl}_2$ .

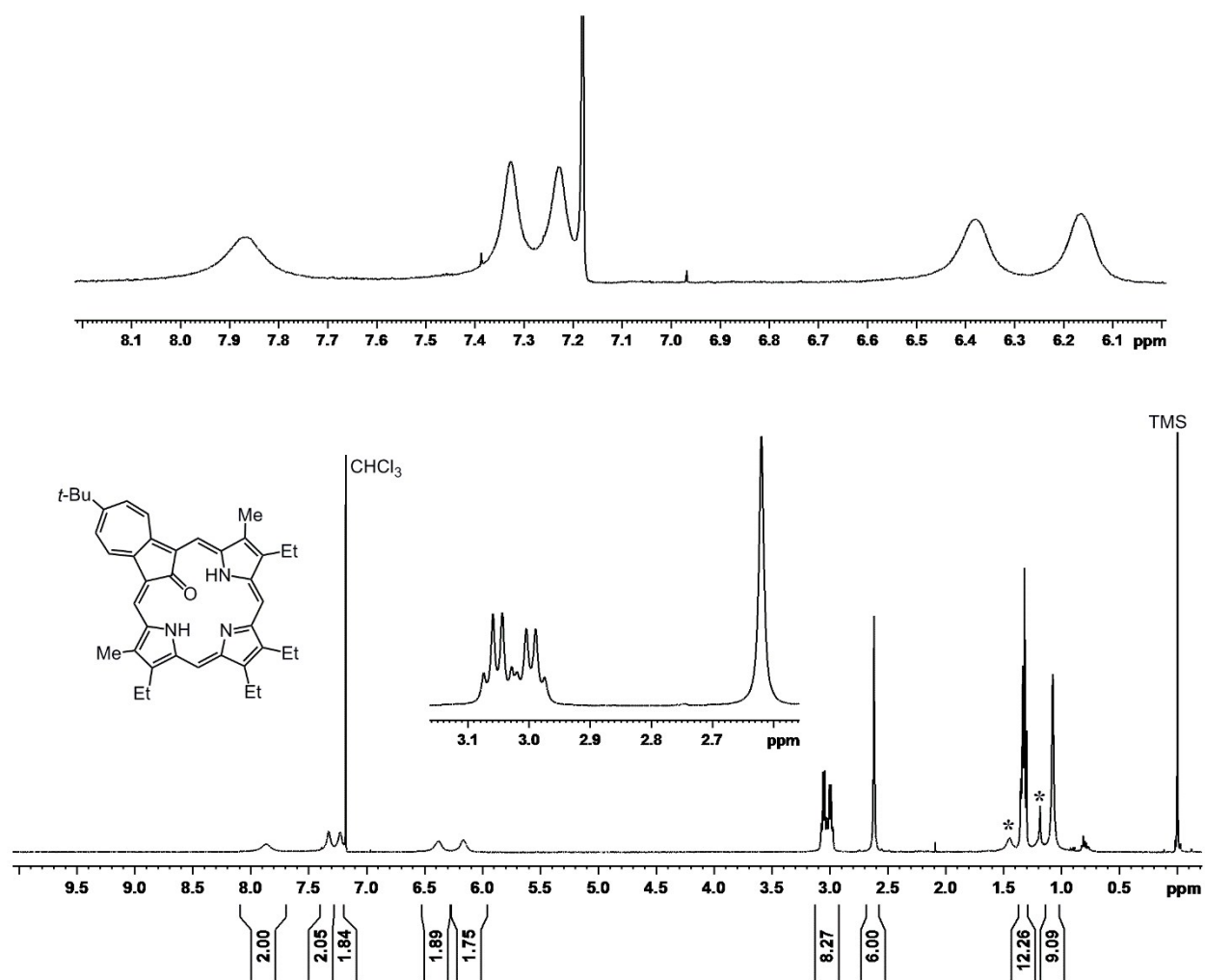


Figure S34. 500 MHz of *tert*-butyl oxyazuliporphyrin **16a** in  $\text{CDCl}_3$  at  $50\text{ }^\circ\text{C}$ .

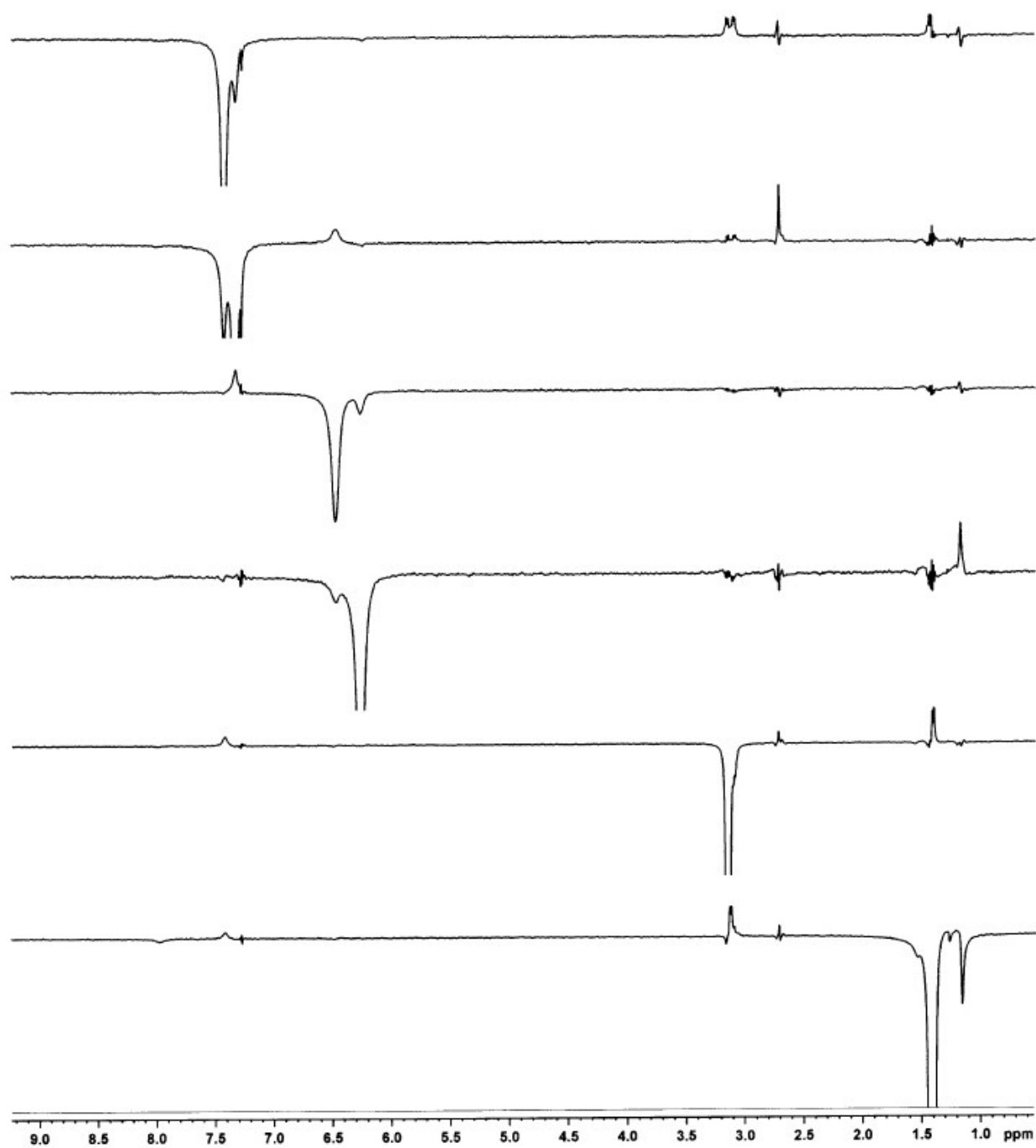


Figure S35. Selected nOe proton NMR spectra of *tert*-butyl oxyazuliporphyrin **16a** in CDCl<sub>3</sub> at 50 °C.

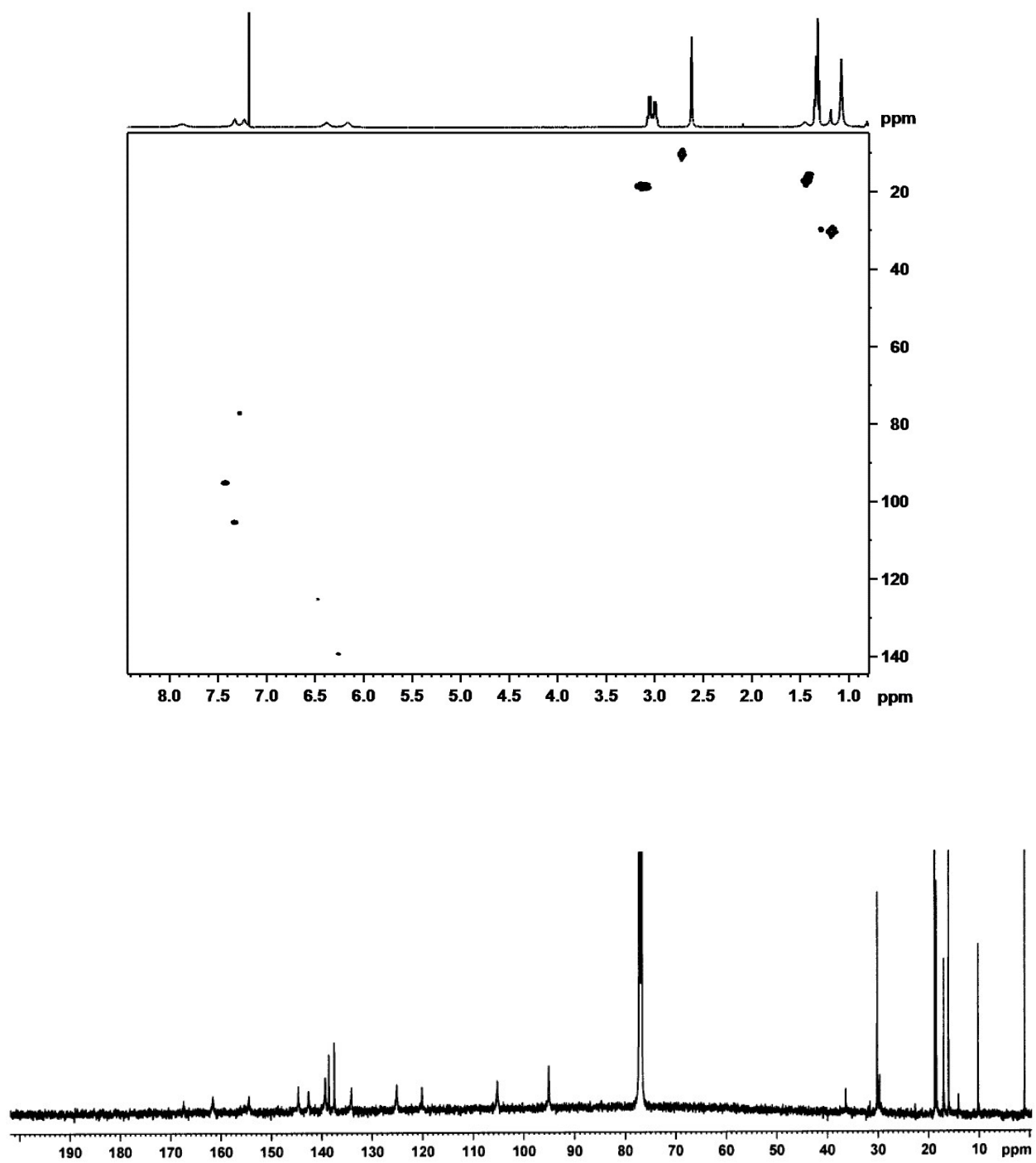


Figure S36. HSQC and 125 MHz carbon-13 NMR spectra of **16a** in CDCl<sub>3</sub> at 50 °C.

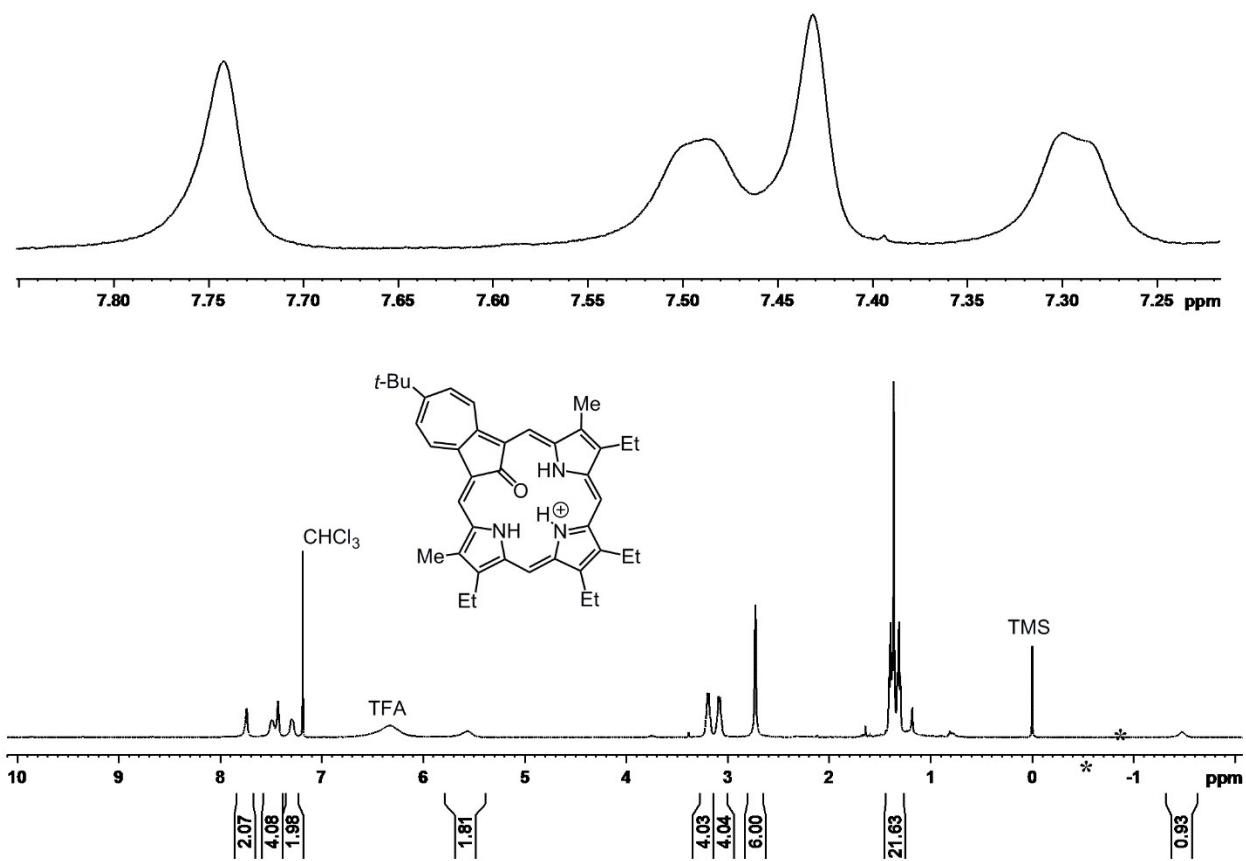


Figure S37. 500 MHz proton NMR spectrum of *tert*-butyl oxyazuliporphyrin monocation **16aH<sup>+</sup>** in TFA-CDCl<sub>3</sub>.

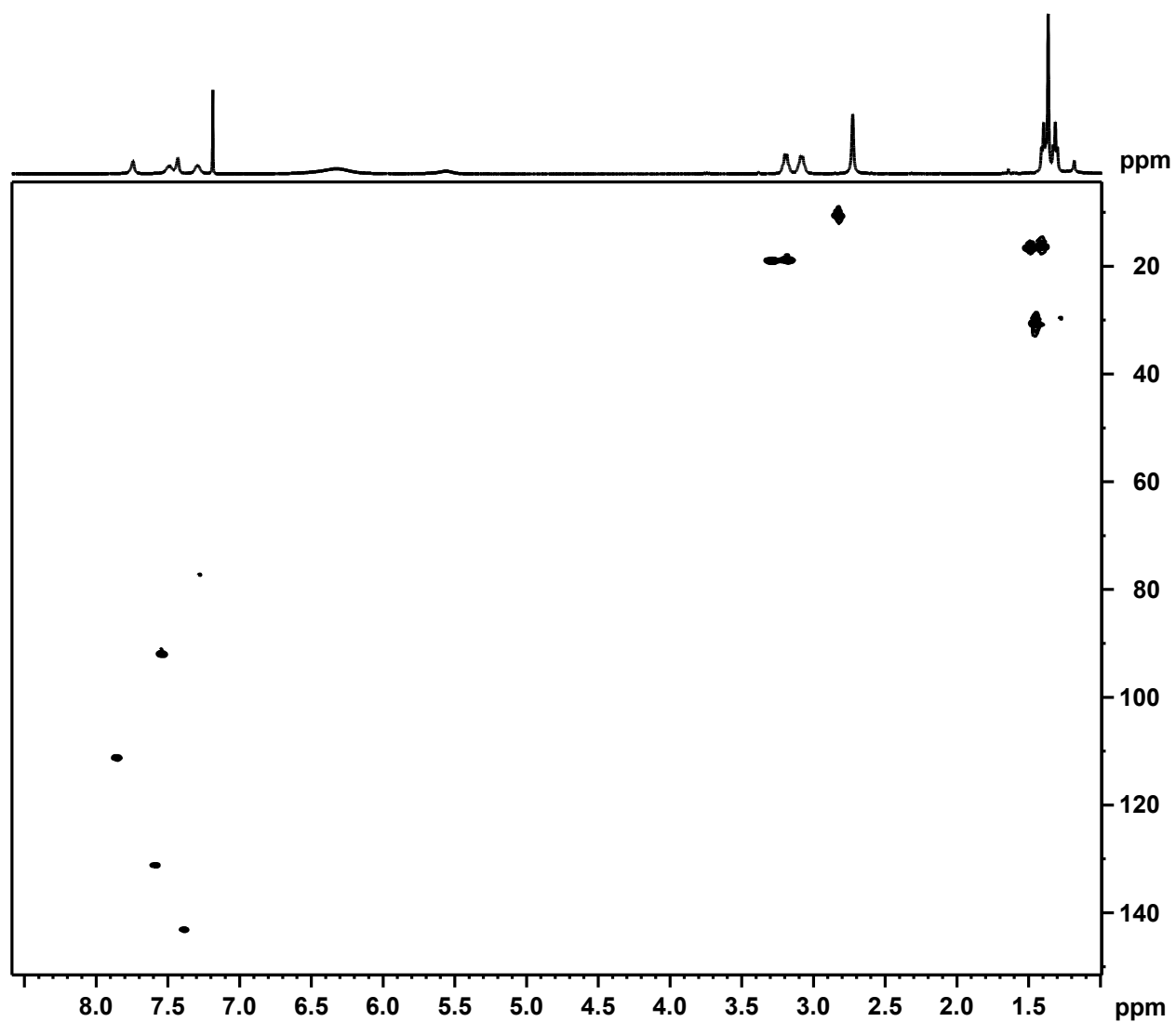


Figure S38. HSQC NMR spectrum of  $16aH^+$  in TFA- $CDCl_3$ .

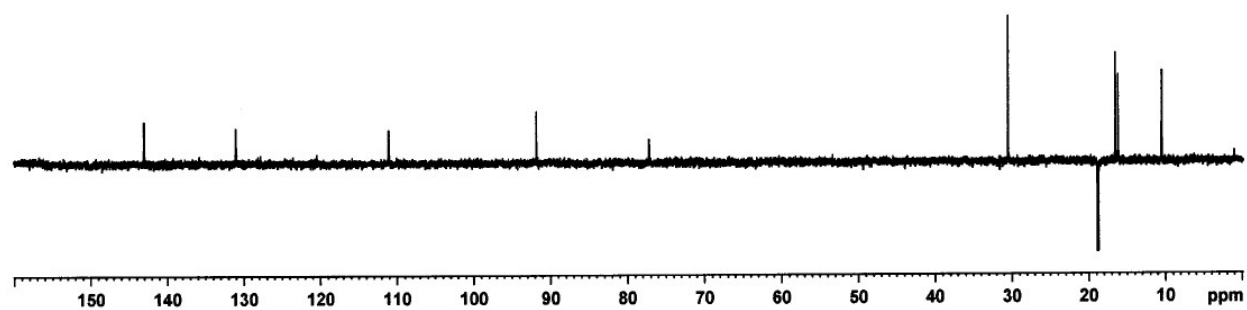


Figure S39. DEPT-135 NMR spectrum of  $16H^+$  in TFA- $CDCl_3$ .

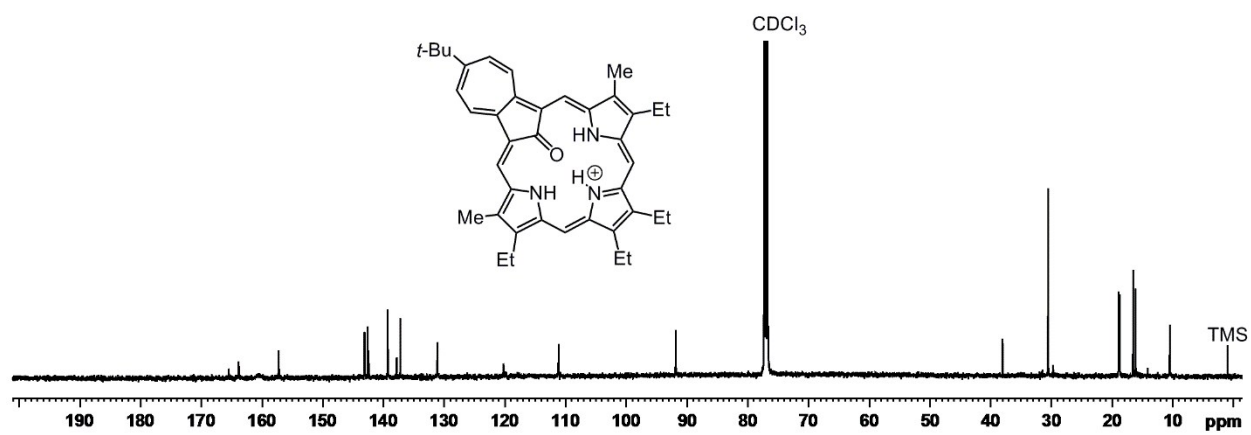
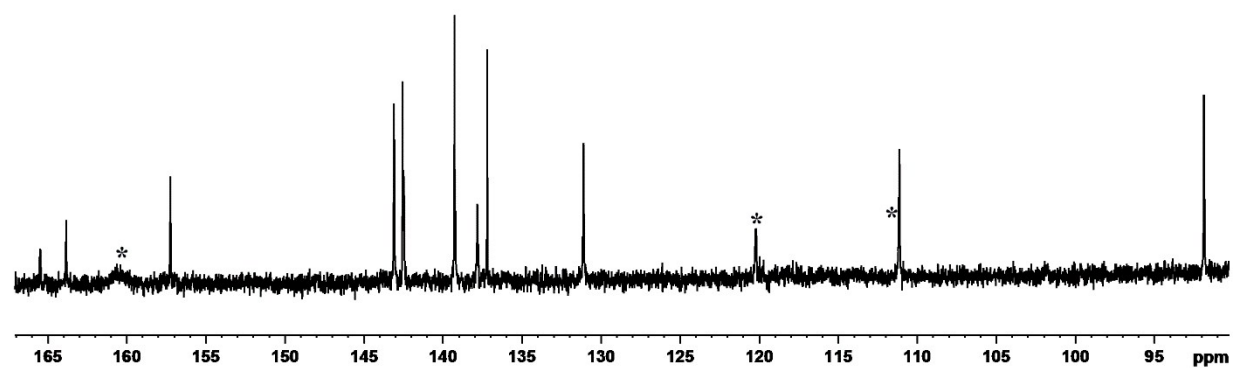


Figure S40. 125 MHz carbon-13 NMR spectrum of **16aH<sup>+</sup>** in TFA-CDCl<sub>3</sub>.

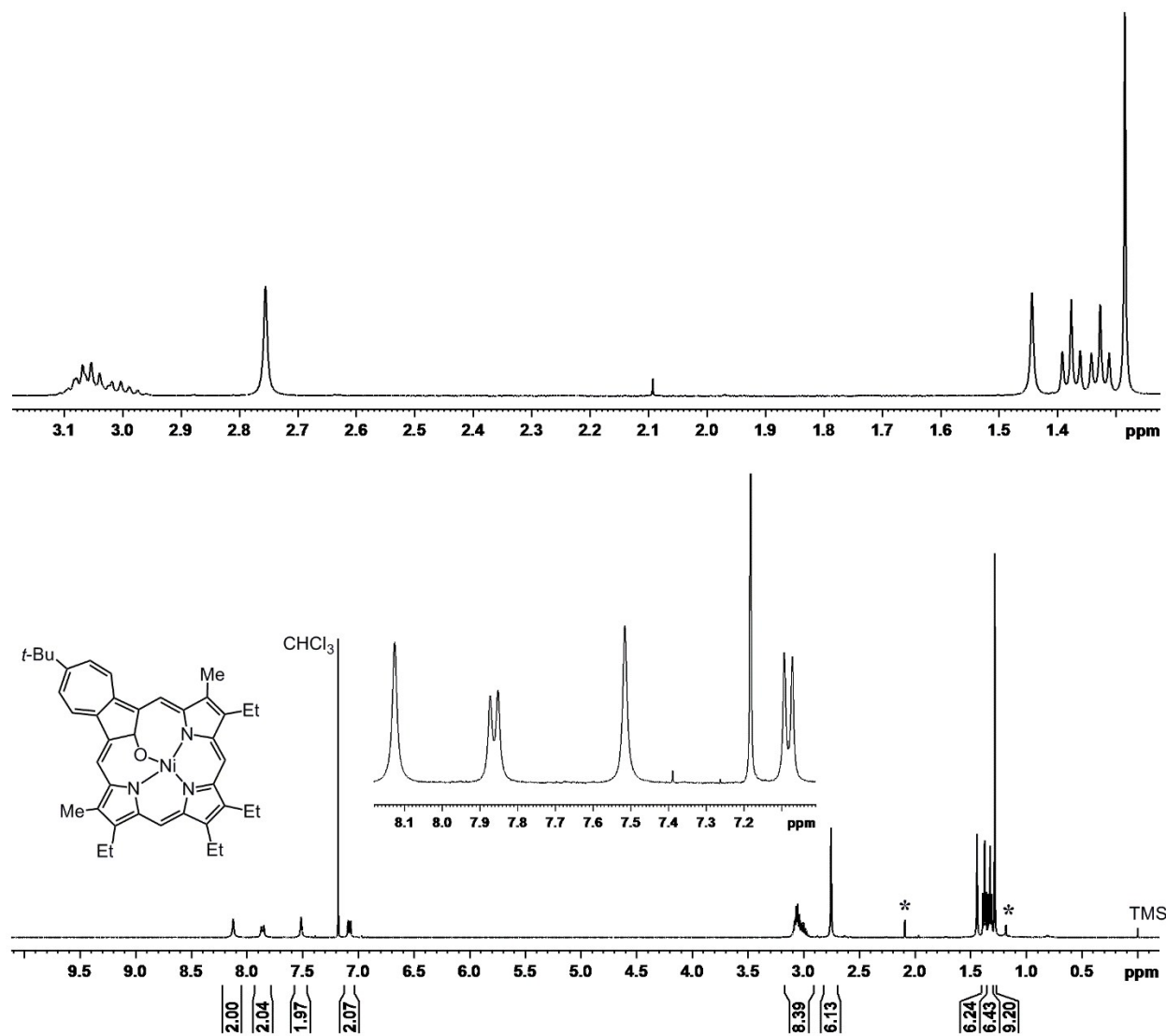


Figure S41. 500 MHz proton NMR spectrum of nickel(II) complex **18a** in CDCl<sub>3</sub>.  
\* solvent impurities

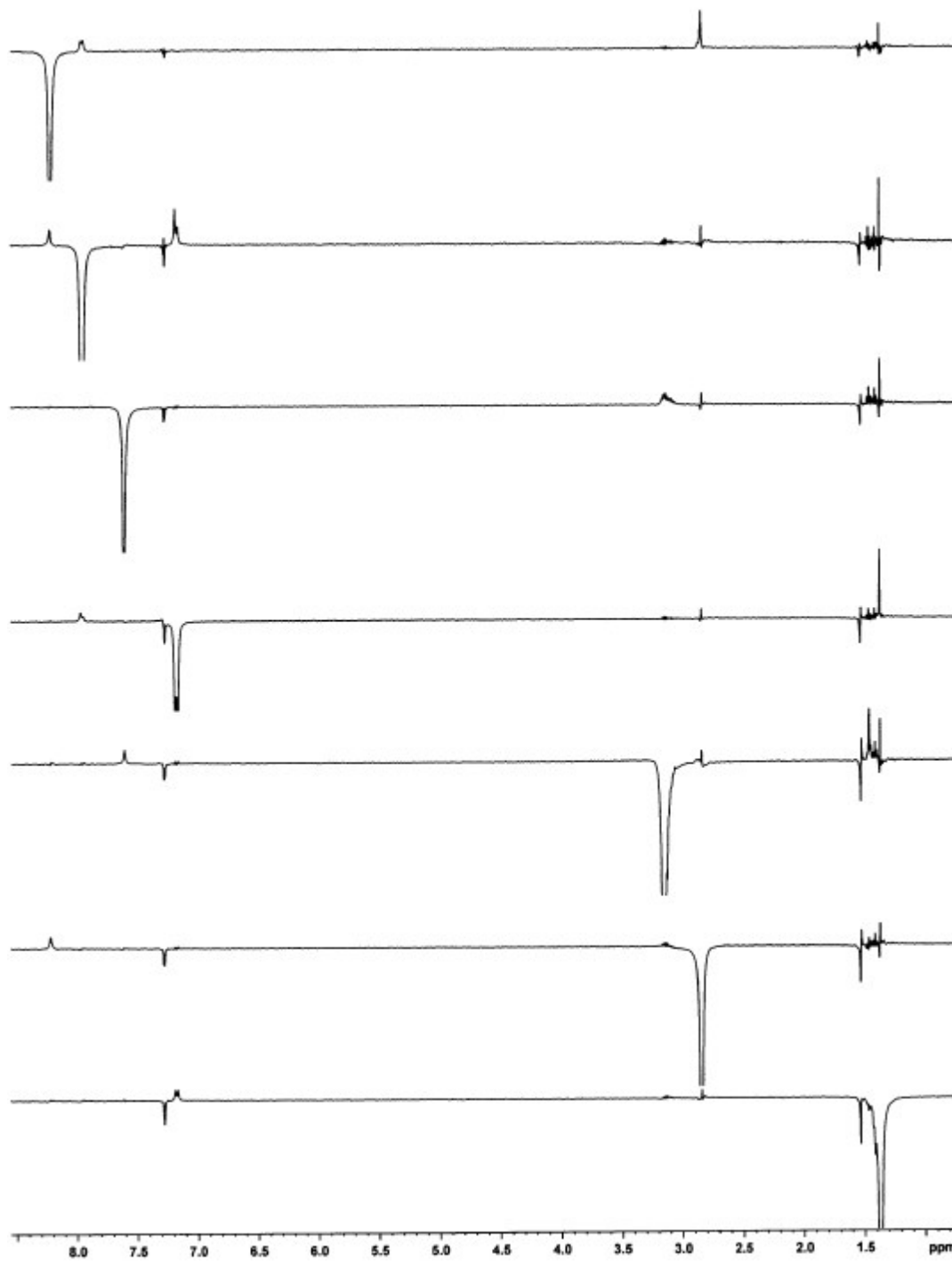


Figure S42. Selected nOe difference proton NMR spectra of nickel(II) complex **18a** in CDCl<sub>3</sub>.

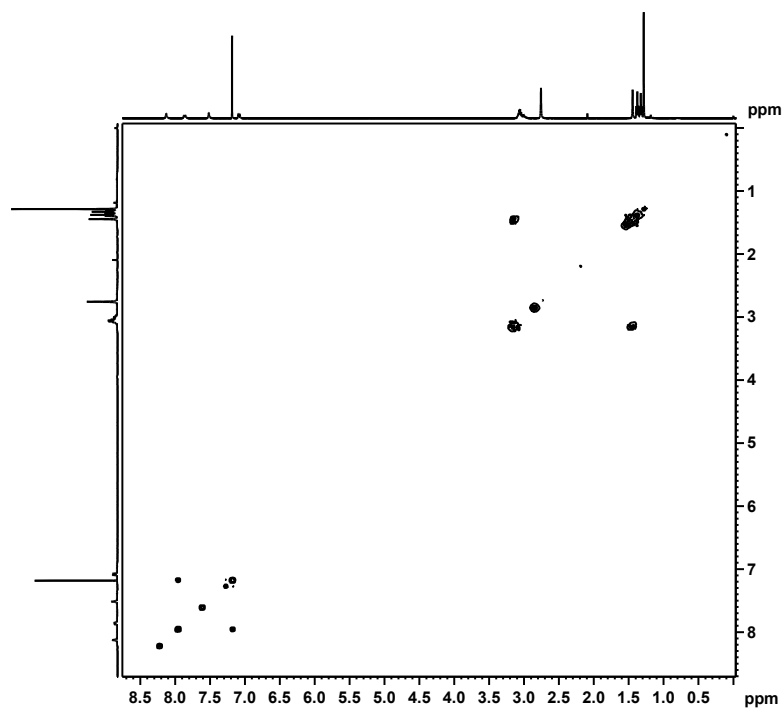


Figure S43.  $^1\text{H}$ - $^1\text{H}$  COSY NMR spectrum of nickel(II) complex **18a** in  $\text{CDCl}_3$ .

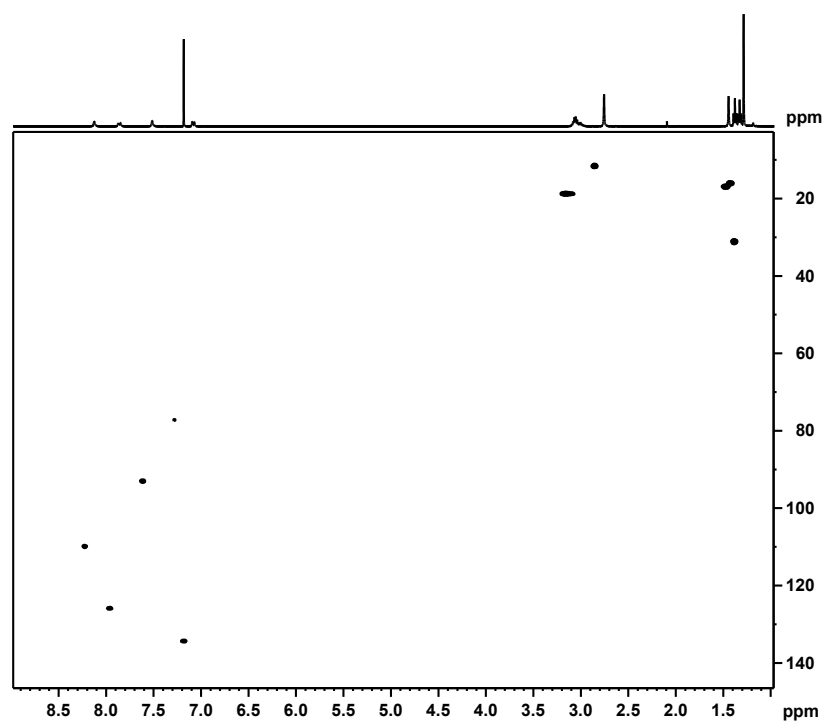


Figure S44. HSQC NMR spectrum of nickel(II) complex **18a** in  $\text{CDCl}_3$ .

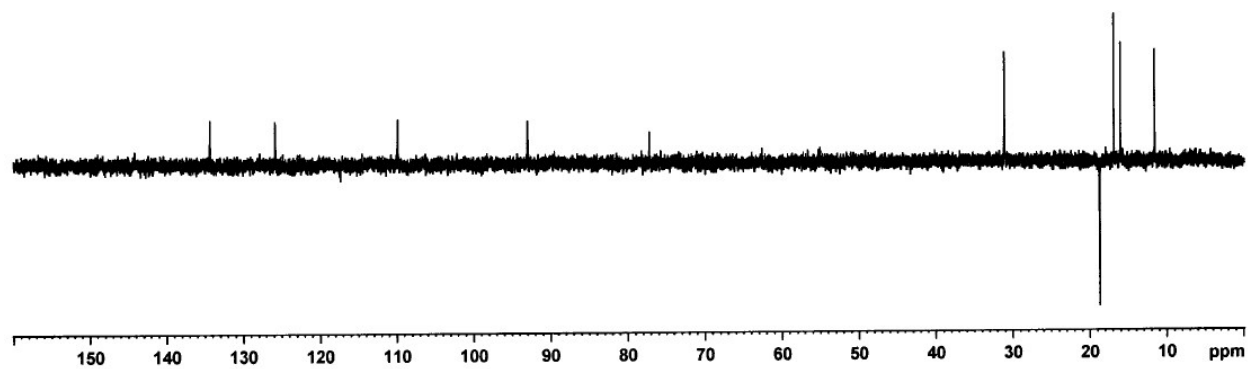


Figure S45. DEPT-135 NMR spectrum of nickel(II) complex **18a** in  $\text{CDCl}_3$ .

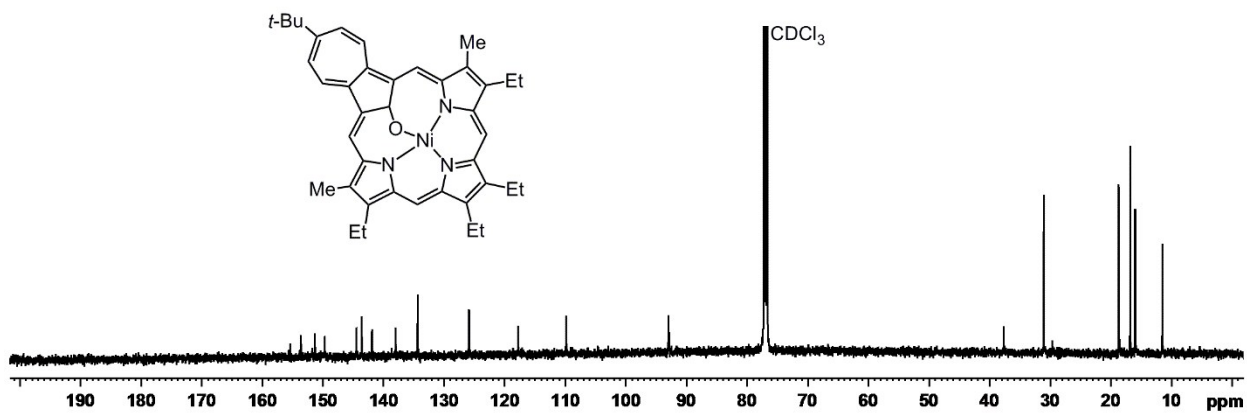
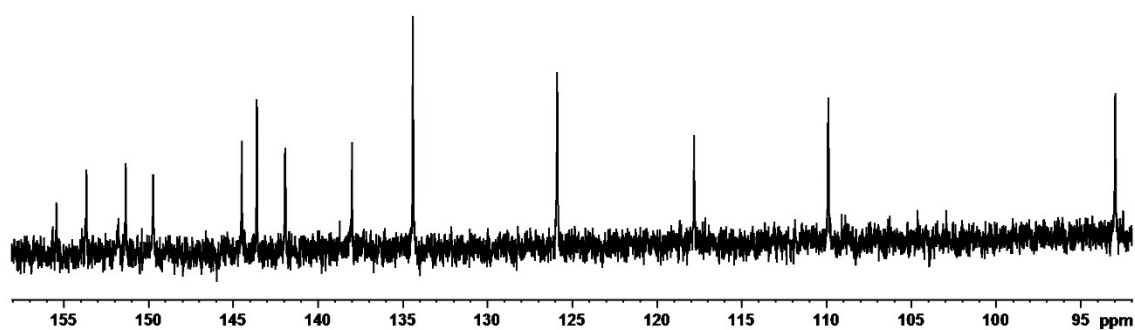


Figure S46. 125 MHz carbon-13 NMR spectrum of nickel(II) complex **18a** in  $\text{CDCl}_3$ .

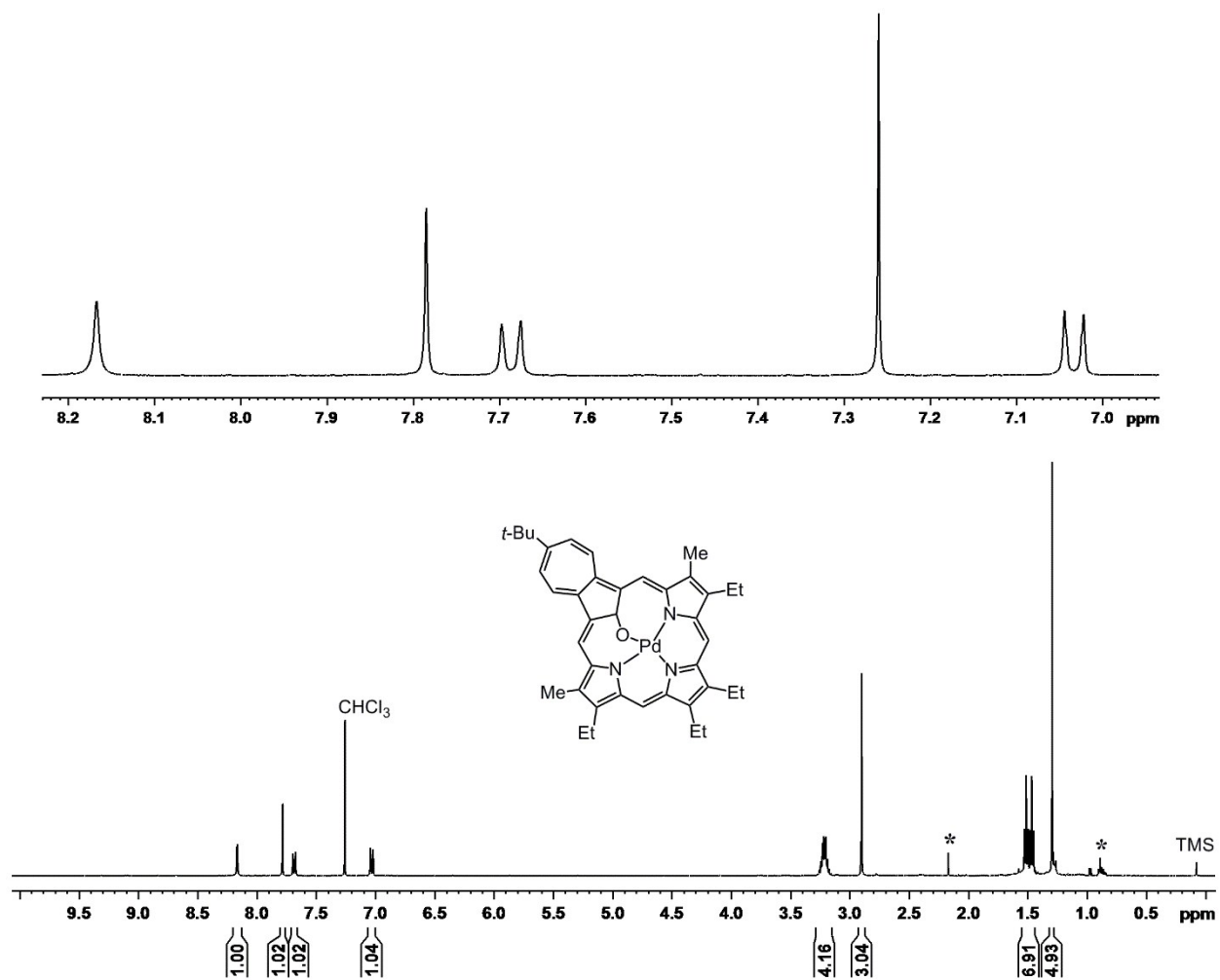


Figure S47. 500 MHz proton NMR spectrum of palladium(II) complex **18b** in CDCl<sub>3</sub>.  
\* solvent impurities

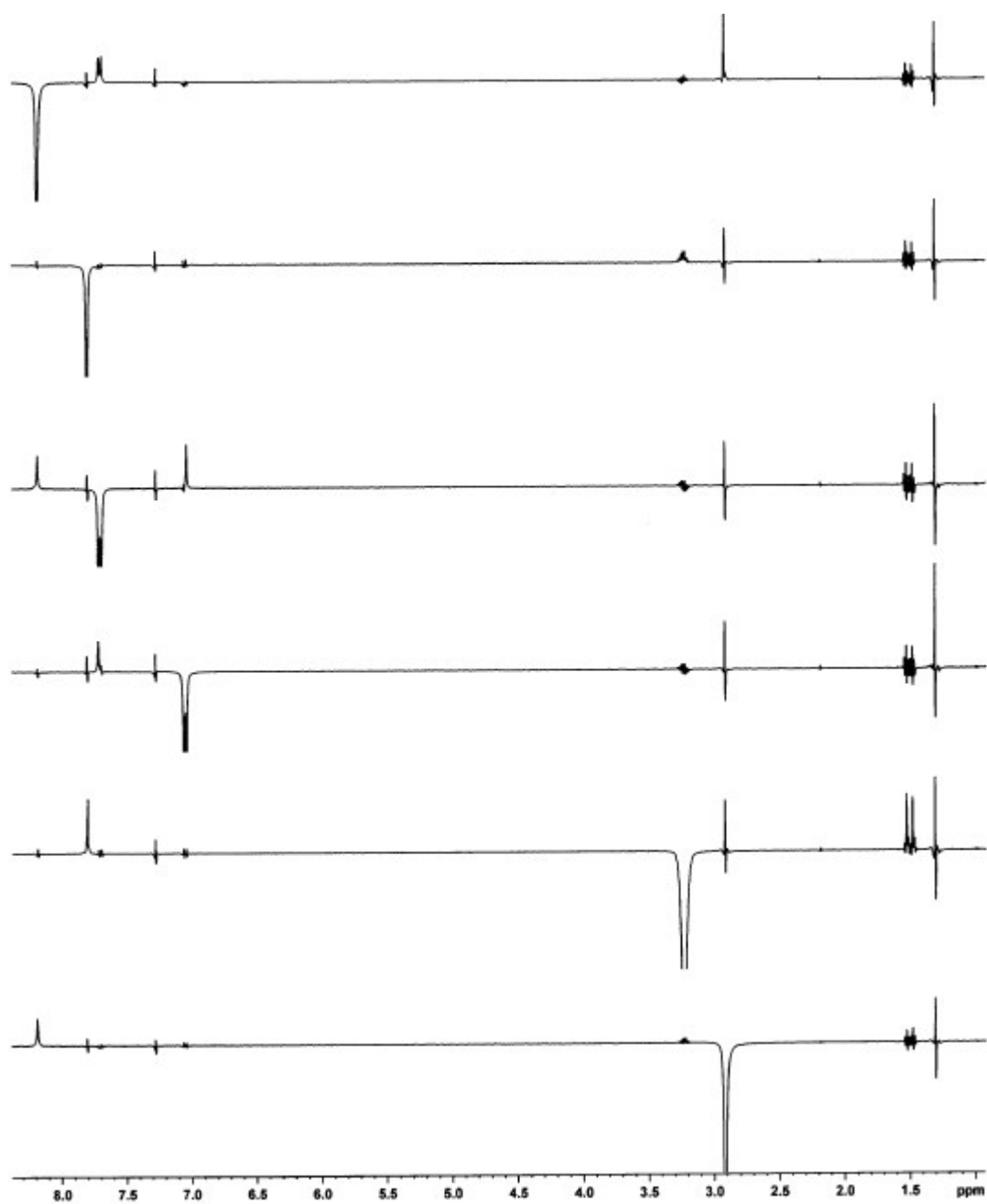


Figure S48. Sected nOe difference proton NMR spectra of palladium(II) complex **18b** in CDCl<sub>3</sub>.

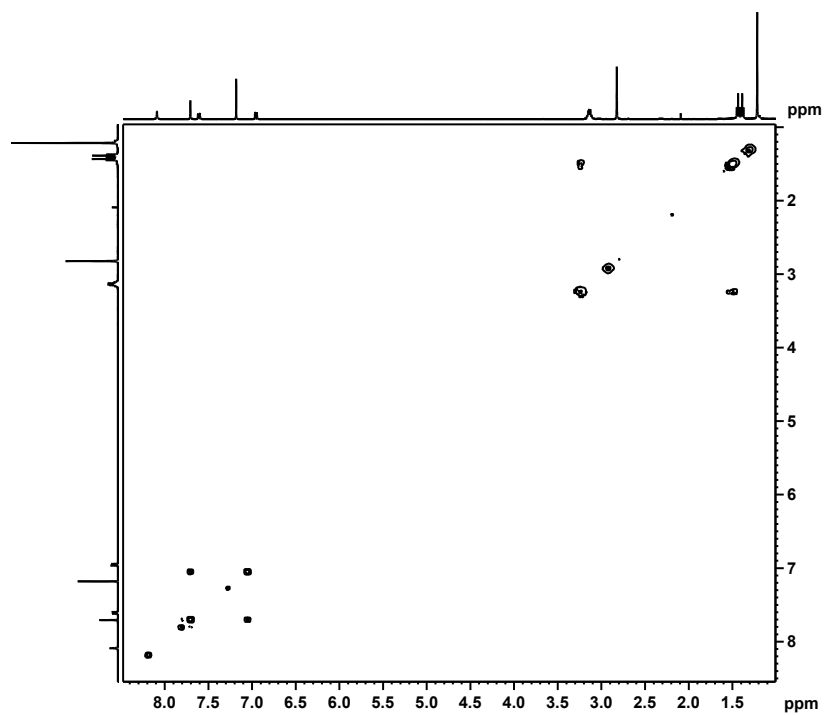


Figure S49.  $^1\text{H}$ - $^1\text{H}$  COSY NMR spectrum of palladium(II) complex **18b** in  $\text{CDCl}_3$ .

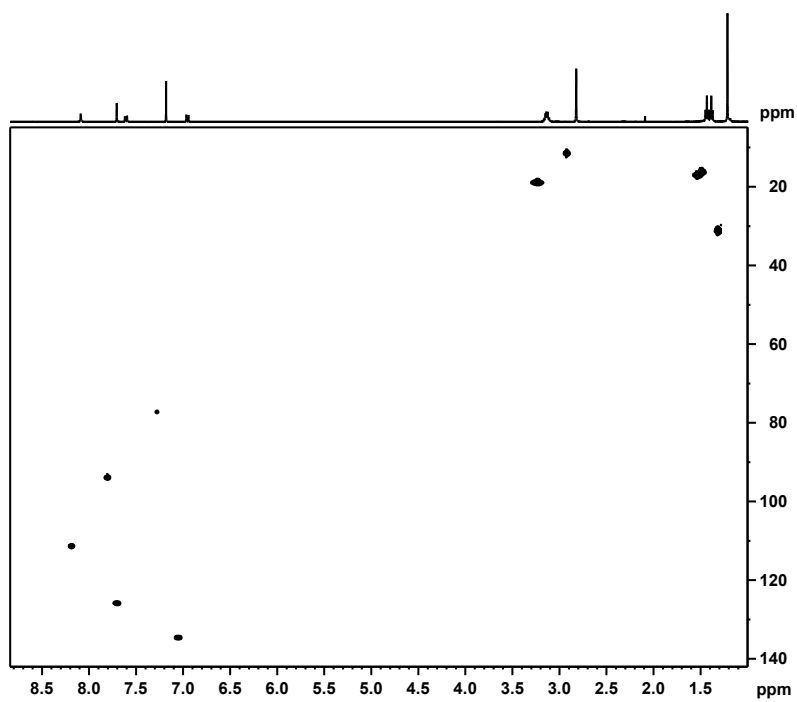


Figure S50. HSQC NMR spectrum of palladium(II) complex **18b** in  $\text{CDCl}_3$ .

